Guard Flow-enhanced Organic Vapor Jet Printing of Molecular Materials in Air

by

Shaurjo Biswas

A dissertation submitted in partial fulfillment
of the requirements for the degree of
Doctor of Philosophy
(Materials Science and Engineering)
in The University of Michigan
2014

Doctoral Committee:

Associate Professor Max Shtein, Chair
Professor Jingsang Kim
Professor Joerg Lahann
Associate Professor Kevin P. Pipe

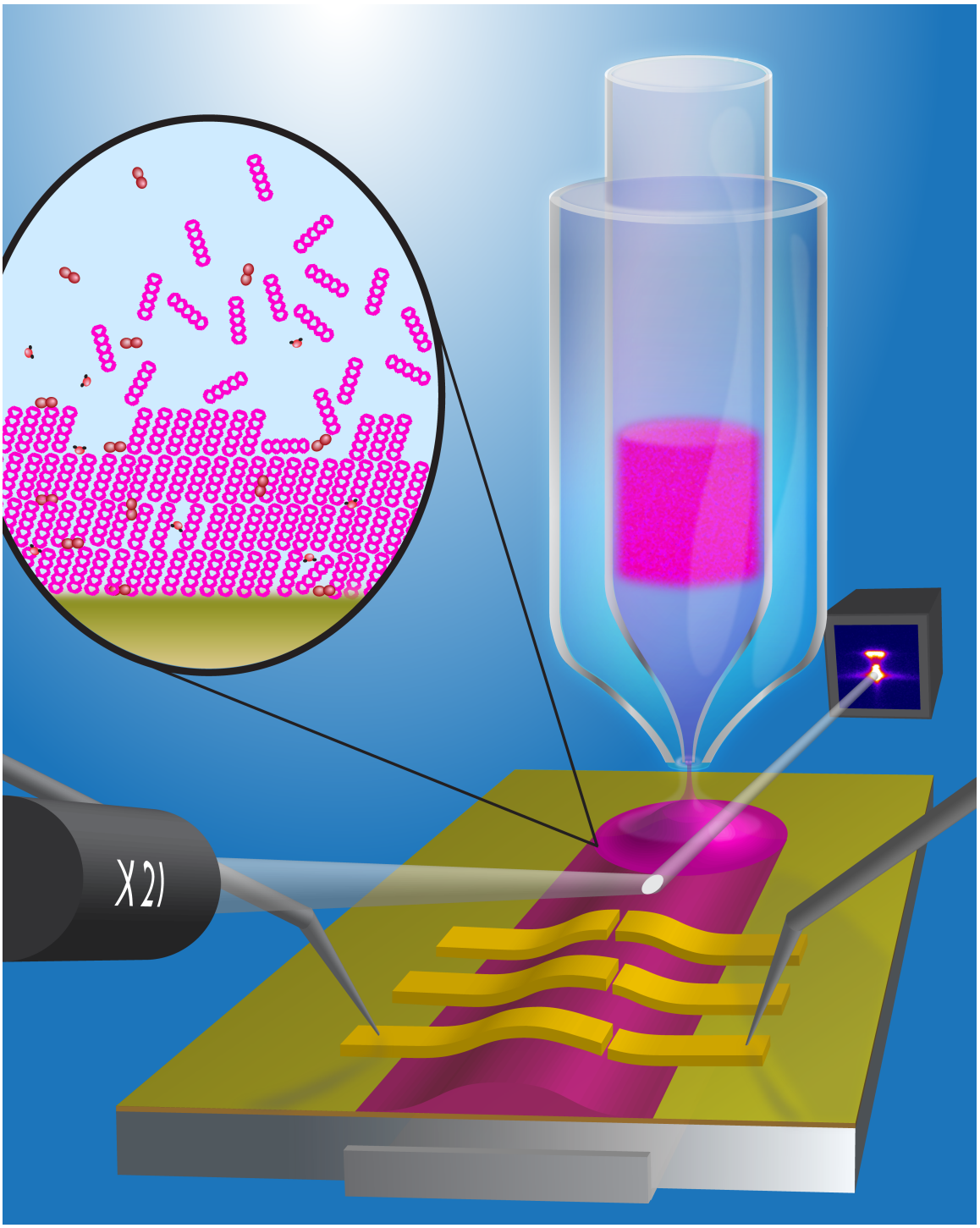
X 21

DEDICATION

This thesis is dedicated to the memory of my beloved mother and closest friend, Antara Biswas. Her love, encouragement and support have made this document possible.

ACKNOWLEDGEMENTS

I would first like to express my sincere gratitude to my advisor, Prof. Max Shtein, who supported me with his patience, motivation, enthusiasm, and knowledge of science and life. His guidance pushed me to strive for excellence in research while giving me the leeway to work in my own way. I could not have wished for a better advisor and mentor. I would like to thank Prof. Kevin Pipe for co-advising me during the first two years of my Ph.D. Without his creative input during the design phase, this work would not have been possible. I would also to thank my other thesis committee members, Prof. Jinsang Kim and Prof. Joerg Lahann for their encouragement, insightful comments and questions. A special thanks to Harald Eberhart, for tirelessly glass-blowing over a hundred nozzles to perfection, bringing my whimsical drawings on paper to reality.

It has been an absolute pleasure to work on GF-OVJP with Olga Shalev and Kyle Luck and other collaborators including Yongsoo Yang, Nadav Geva, Christian Schlepütz, Tamir Arbel and David Hinz. I am grateful to my fellow students and lab members who I've worked beside over the course of my doctoral research for providing many stimulating and intellectual discussions, assistance with research and making my work and stay in Ann Arbor enjoyable, including Kanika Agrawal, Kwang Hyup An, Adam Barito, Paddy Chan, Mark Hendryx, Yansha Jin, Gwan Ho Jung, Steven Morris, Denis Nothern, Brendan O'Connor, Olga Shalev, Matthew Sykes, Abhishek Yadav, Yiying Zhao, and many

others. I am especially indebted to Steve and Yansha for growing up and growing old with me in the lab, Denis and Matt, along with Diana Sykes, for the many many after-hours 'therapy' sessions and Olga, whose work ethic, intelligence and compassion have been an inspiration.

My heartfelt appreciation goes out to my flatmates, Shiladitya Sen and Titli Maitra, for putting up with my crazy work hours, cooking the most delicious food and all the help and support during good times and bad. They will remain my lifelong friends. Last, but not the least, I am eternally thankful to my family – my father and brother, Siddhartha and Shirsho Biswas, for their absolute love and encouragement, and my wife, Debaleena Basu, who has been a pillar of strength and outrageously loving and supportive in our long-distance marriage during my Ph.D.

TABLE OF CONTENTS

LIST OF FIGURES

Figure

ABSTRACT

Rapid advances in the research and development of organic electronics have resulted in many exciting discoveries and applications, including organic light emitting devices (OLEDs) for information display and illumination, organic photovoltaic (OPV) devices, photodetectors, chemosensors, organic thin film transistors (OTFTs) and memory. Small molecular organic optoelectronic devices often call for sharp interfaces and highly pure materials for improved device performance. Solvent-free deposition and additive patterning of the active layers is preferred, calling for specialized processing approaches. Several deposition and patterning methods for small molecular thin films and devices have been developed, including vacuum thermal evaporation (VTE), organic vapor phase deposition, and organic vapor jet printing, but the dominant approach used today – vacuum thermal evaporation with movable shadow masks – does not scale up easily.

Guard flow-enhanced organic vapor jet printing (GF-OVJP), however, enables additive, rapid, solvent-free printing of molecular semiconductors in ambient atmosphere by evaporating organic source material into an inert carrier gas jet, which impinges onto a substrate where the organic molecules condense. A surrounding annular "guard flow" focuses the primary jet and shields it from contact with the ambient oxygen and moisture, enabling device-quality deposition in air. The technique is compact and scalable. This thesis demonstrates the deposition of

active layers of OLEDs, OPVs, OTFTs by GF-OVJP in air. Process-structure-property relationships are elucidated, using a combination of film deposition and structural characterization, device fabrication and testing, as well as compressible fluid flow, heat and mass transport modeling.

Firstly, a fluorescent material, AlQ_3, is printed by GF-OVJP in air to form the active layer of an archetypal, bi-layer OLED comparable device properties as those fabricated by VTE. Process parameters are optimized to improve devices performance and pattern resolution. Next, GF-OVJP is used to grow donor (SubPc) and acceptor (C_{60}) films in air for standard and inverted OPV device applications, revealing that film crystallinity and roughness can be affected greatly by the guard flow, potentially enhancing cross-plane carrier transport / exciton and photovoltaic device performance. Thirdly, dry printing in air is demonstrated of various organic semiconductors (pentacene, tetracene, DNTT) for application as OTFT channels. Synchrotron XRD and AFM are used to characterize the growth dynamics and the resulting film structure, complemented by measurement of electronic properties of GF-OVJP deposited films in TFTs, establishing a quantitative process-structure-property relationship. Finally, GF-OVJP technique is modified to enable surface polymerization of parylene. The air-deposited parylene layer is shown to increase the lifetime of an encapsulated OLED.

This thesis thus lays the groundwork for rigorous, quantitative design of film deposition apparatus and small molecular organic semiconductor processing.

CHAPTER 1

Introduction

1.1. Background and motivation

Conjugated molecular organic compounds have received increasing amounts of attention in the scientific and engineering communities for their applications in solar energy conversion, efficient solid-state lighting, flexible electronics, and other areas. From the earliest reports of the photovoltaic effect in organic thin films [1, 2] to the recent commercialization of organic light-emitting devices (OLEDs) for flat-panel displays, progress in the field of organic optoelectronics has been rapid. OLED external quantum efficiency (EQE) exceeding 20% [3] and luminous power efficiency of more than 100 lm/W [4] were shown, organic photovoltaic power conversion efficiency of over 10% [5] was achieved, and field-effect mobility in organic transistors was improved beyond 5 cm^2/V-s [6]. The concurrent development of materials and device structures enabled exquisite control over charge injection, transport, and recombination; exciton transport; and light in- or out-coupling. Meanwhile, to transform the organic semiconductor compounds from their initial state (typically, purified crystalline powder) into multilayered device structures over large areas, a remarkably small set of processing techniques have been deployed [mostly vacuum thermal evaporation (VTE)]. A review of these techniques has been published by Biswas *et al*. [7] and forms the basis of this chapter.

The focus of this thesis is on van der Waals–bonded, small–molecular weight (e.g., smaller than ~10^3 g/mol) organic compounds, some of which are shown in **Fig. 1-1**. The relatively weak intermolecular forces [8] enable the nonepitaxial deposition [9] of high-quality thin films on a range of substrates, including glass and flexible plastics. However, the nature of bonding in these materials typically restricts processing to nonreactive and dry techniques. For example, sputtering finds limited application due to the fragility of the organic thin films under ion bombardment, whereas use of conventional photolithography is restricted by the films' high permeability by common solvents. Furthermore, solvent-based deposition methods face the difficulty of adjusting the solubility of individual components independent of their optoelectronic properties.

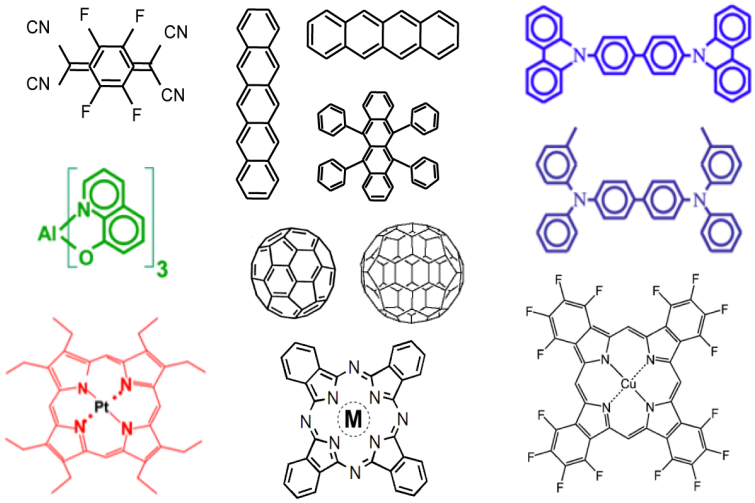

Figure 1-1 Small molecular organic semiconductor materials: chemical structures of the conjugated organic and organometallic compounds of interest in optoelectronic device applications. They include archetypal electron- and hole-transport materials, wide band-gap hosts, dopants, electron donors, acceptors, and sensitizers. [7]

A variety of techniques have been developed to enable the precise deposition and patterning of molecular organic thin films, geared toward device fabrication. Here, some of these techniques like vacuum thermal evaporation (VTE), organic vapor phase deposition (OVPD), organic vapor jet printing (OVJP), laser-induced thermal imaging (LITI), and active-layer patterning by shadow masking and transfer methods are briefly discussed. Industrial application of these deposition methods brings up special engineering challenges concerning material utilization efficiency, pixel crosstalk, apparatus contamination, takt time, and many other factors, which are also relevant to the art of thin-film growth in a research setting. Of particular interest are methods that enable additive patterning of active layers involved in charge and exciton transport, light absorption or emission, and other important functions in devices. Substantial interest persists in developing improved techniques for optoelectronic device deposition and patterning in the ambient, in part due to the potential for cost reduction and environmental benefits when compared to conventional vacuum- or solvent- based processing. Guard flow-enhanced organic vapor jet printing (GF-OVJP) is one of the solutions developed to address these issues. [7]

OVJP enables direct patterning of the active organic layers, and is the basis for the GF-OVJP method, which is the focus of this thesis. Briefly, an inert carrier gas (e.g., nitrogen, helium, argon, etc.) picks up organic vapor and impinges as a collimated jet onto a substrate, where the heavier organic molecules selectively condense. [10] However, when applying the same process to deposit in air, a significant limitation arises; the hot organic vapor mixes with the surrounding oxygen and moisture en route to the substrate. Because the highly conjugated organic semiconductor compounds are susceptible to oxidative damage at elevated temperatures, their device-relevant properties usually degrade

in air, lowering device performance. To address the limitation described above, the primary jet is concentrically surrounded with a secondary jet of inert gas, reducing pattern dispersion and protecting the organic vapor from the surrounding atmosphere. [11]

This thesis attempts to explore the potential of GF-OVJP as a viable technique to deposit and pattern device-quality, organic thin films in air for various optoelectronic applications. To evaluate the contribution of GF-OVJP to the fabrication space, it is necessary to understand the principles of molecular optoelectronic devices and examine some of the existing deposition techniques mentioned above along with their advantages and drawbacks.

1.2. Small Molecular Organic Semiconductor Devices

Interest in organic electronics stems from a combination of intriguing electronic and optical properties of the materials, coupled with the ability to deposit organic films on a variety of low-cost substrates, such as glass, plastic, or metal foils, as mentioned in the introduction. OLEDs for flat-panel, information-display applications have enjoyed the most rapid improvements [12], propelled by the value-added nature of the application, for which the rich color gamut and energy efficiency afforded by organic emitters are highly desirable. High-efficiency, very bright and colorful thin displays based on OLEDs are in commercial production by several manufacturers. Advances in organic electroluminescence for display applications are paving the way for OLED-based solid-state lighting, where the new technology must compete with multiple established paradigms (e.g., incandescent, fluorescent, and inorganic LED-based lighting).

Significant progress is also being made in the realization of organic thin-film transistors (OTFTs) [13] and thin-film organic photovoltaic cells (OPVs) [14] for cost-effective and ubiquitous electronics and solar electricity generation. The cost of semiconductor layers used in most thin-film solar cells is low, so the ultimate success of organic semiconductors in these applications likely depends on leveraging the ability to integrate devices on inexpensive, large-area substrates using very low-cost, low-energy-intensity [15], high-throughput production techniques. To provide context for the discussion of OLED, OTFT, and OPV device-fabrication methods, The structure, operating principles, and performance characteristics of the devices themselves are briefly discussed below.

1.2.1. Organic Light-Emitting Devices

Although basic electroluminescence in an organic compound was demonstrated as early as 1953 [16] and 1965 [17], it wasn't until Tang & VanSlyke's [18] 1987 demonstration of the first heterojunction OLED that the science and technology of OLEDs began to gain momentum. High efficiency, archetypal heterojunction OLEDs [18, 19] typically comprise organic layers sandwiched between two thin film electrodes, as shown in **Fig. 1-2**. Electrons and holes injected under electrical bias from the cathode and anode, respectively, undergo drift diffusion through the respective transport layers and recombine at the interface, emitting heat and light. To first order, the thicknesses and composition of the individual layers dictate the amount of injected charge for a given voltage as well as the overall efficiency of the OLED. The color of emitted light is controlled primarily by choosing an appropriate HOMO-LUMO energy gap of the dopant molecules placed at the interface between the electron- and hole-transporting layers. Confinement of excited states (excitons) is a key consideration, accomplished through the use of large-

energy-gap, exciton-blocking layers that can increase the probability of radiative recombination of excitons away from the quenching electrodes.

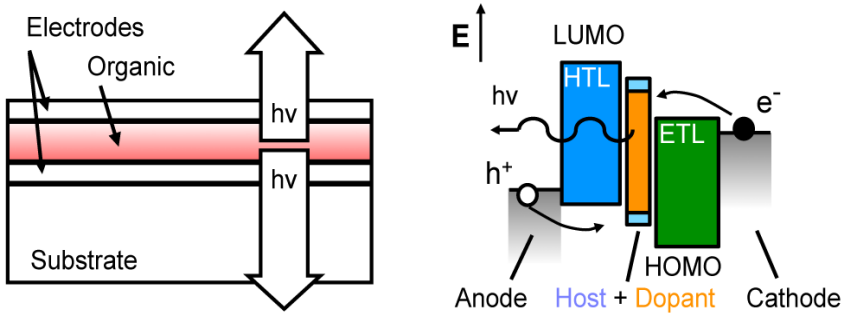

Figure 1-2 A schematic of an organic light-emitting device (OLED) structure, showing organic layers sandwiched between two electrodes, at least one of which is transparent. Also shown is an energy-level diagram for a device consisting of anode, hole- and electron-transport layers (HTL and ETL), doped emissive layer (i.e., consisting of two or more components), and cathode. Holes and electrons are injected and recombine in the emissive layer. Interfaces and doping are important in this structure for balancing current injection, localizing recombination, and increasing emission efficiency. [7]

Several definitions of efficiency are associated with lighting devices, including EQE (measured in %) and luminous and power efficiencies. EQE is the ratio of the number of photons emitted to the number of electrons injected into the device; luminous efficiency, η_L, is similar to EQE, except that η_L convolves the number of emitted photons normalized by the photopic response of the eye (most sensitive in the green portion of the visible spectrum) and is measured in candelas per amp (cd/A). Power efficiency is typically quoted in lumens per watt of power used to drive the device and is important in determining the cost to operate a light source. The EQE can be represented as a product of the efficiencies of individual steps leading to light emission from the OLED:

$$EQE = \eta_{inj} \cdot \eta_{xport} \cdot \eta_{rec} \cdot \eta_{rad} \cdot \eta_{out} \quad (1.1)$$

where η_{inj} is the charge-injection efficiency, η_{xport} is the charge-transport efficiency, η_{rec} is the charge-recombination efficiency (or charge balance factor, often written as γ), η_{rad} is the radiative efficiency (<0.25 for electrofluorescence or <1 for electrophosphorescence [20, 21]), and η_{out} is the light outcoupling efficiency (typically <0.5 [19, 21]). State-of-the-art electrophosphorescent devices can achieve $\eta_{rec} \cdot \eta_{rad}$ approaching 100%, whereas η_{out} in some device configurations can be 50%.

Any candidate deposition technique must help extract the maximum potential from the materials comprising the device. Current density-voltage-light (J-V-L) characteristics are measured, along with the electroluminescence spectra of OLEDs, to quantify device performance [22]. The J-V characteristic of an OLED typically exhibits two distinct regimes: space-charge limited (SCL) and trapped-charge limited (TCL). In the SCL regime, $J \propto V^2$. In the TCL regime, carrier mobility is limited by trapping of carriers in deep and shallow energy levels in the film, which arises from a combination of impurities, damaged material, and disorder. Increasing electrical bias on the electrodes floods the films with charge, which fills the finite number of traps and causes a rapid increase in the effective carrier mobility. As a result, a rapid, power-law increase in cur- rent is observed, governed by thermally activated, variable range hopping, with $J \propto V^m$, where $m > 7$. At sufficiently high injection levels, all the traps are filled, reaching the trap-filled limit, and consequently the current again becomes SCL [23].

Many organic semiconductor compounds, as well as their interfaces with electrodes in devices, can degrade rapidly in air. Studies on OLEDs [24, 25] show two main degra-

dation pathways: long-term intrinsic decay in the electroluminescence intensity, which leads to a uniform loss of efficiency across the light-emitting surface, and faster degradation through formation and growth of nonemissive regions or dark spots, which are attributed to regions of poor electron injection formed by local oxidation. Continuous diffusion of oxygen and water into the device leads to growth of the oxidized region of the cathode, which expands radially from the defect (e.g., a pinhole in the electrode).

Two primary architectures have emerged for realizing full-color information displays based on OLEDs. In one approach, the basic RGB pixel triad (or pentile pattern) is achieved by patterning the red-, green-, and blue-emitting OLEDs side by side, which requires at the very least the in- plane patterning of each emitter with edge definition on the order of 20 micrometers or better, depending on the type of display. In another approach, the OLED component takes the place of a conventional backlight coupled with switched liquid crystal–based red, green, and blue filters. In the latter configuration, the patterning requirements for the organic emitters can be relaxed, although the energy efficiency and color gamut are in principle inferior to the first approach. In either case, the active organic layers are usually deposited by VTE, and pixilation is achieved by using a shadow mask. It has emerged that shadow masking severely limits the scalability of OLEDs, increasing the urgency for low-cost, scalable, direct patterning, which is covered in a subsequent section.

1.2.2. Organic Photovoltaic Cells

As an intrinsically large-area and cost-driven application, solar cells benefit from the strong light absorption of organic dyes and the ability to rapidly deposit device-quality organic semiconductor thin films at ambient conditions on a variety of substrates without

the need for lattice matching. The photovoltaic effect in organic films was observed as early as 1958 [1] and was followed by reports on Schottky junction–based organic photovoltaics [26]. The efficiency of these early devices was extremely low, in part due to suboptimal absorption and the inability to dissociate strongly bound electron-hole pairs by the weak built-in field of Schottky junctions. A breakthrough by Ching Tang [2] was to design a heterojunction, in which two different organic materials were used to create a functional analog to the classical semiconductor *p-n* junction. Similar to OLEDs, the EQE of organic solar cells can be represented as a product of the intermediate step efficiencies, including those for light absorption that generate molecular excitons, exciton diffusion, and exciton dissociation across the donor-acceptor interface and eventually charge extraction to the electrodes. To address an inherent tradeoff between light absorption and exciton diffusion in organic thin films, bulk heterojunction architectures were developed [27]. At the time of this writing, the power conversion efficiency of organic solar cells exceeds 11%, and several efforts worldwide are directed toward scale-up and commercialization for a range of applications where flexibility and light weight are advantageous [28]. Compared with many other (inorganic) solar cell technologies, organic-based PV cells potentially offer some of the shortest energy payback times [15]. Note, however, that to reduce solar photovoltaic module installation costs, efficiency must be maximized, and the methods used for large-scale production of solar cells must result in stable, efficient device structures.

The reader is referred to excellent reviews of organic photovoltaic device physics and material selection [29, 30]; some considerations are briefly discussed here to contextualize OPV device-processing challenges and approaches. Nearly identical to the structure

of heterojunction OLEDs, an archetypal heterojunction OPV cell consists of organic thin films sandwiched between two electrodes, one of which is transparent. Typically, the substrate is glass or plastic, precoated with a transparent conducting metal-oxide anode or thin conductive metal, and the cathode is a thick metal reflective layer. The thin (<200-nm) active organic layer comprises at least two materials with different LUMO (and/or HOMO) energy levels, which form a planar or inter-digitated heterojunction. As noted above, light absorbed in these layers forms excitons, which diffuse randomly inside the organic layers. Parasitic quenching of excitons can occur in the bulk, at the electrodes, and by energy transfer to other moieties inside the material. Upon encountering the donor-acceptor heterojunction, excitons can dissociate into interfacially bound polaron pair states, which precede the generation of more spatially separated electrons and holes that can be subsequently collected at the electrodes. Increased molecular order affects the thermodynamics and kinetics of these processes and can thereby improve energy and charge transport considerably, which boosts the overall power conversion efficiency [31–33].

Some of the important parameters for characterization of OPVs (indicated in **Fig. 1-3**) include short-circuit current (J_{SC}, measured in mA/cm), open-circuit voltage (V_{OC}, measured in V), fill factor (FF), and the overall power conversion efficiency (η_P). Various materials and device architectures have been employed to improve these characteristic parameters.

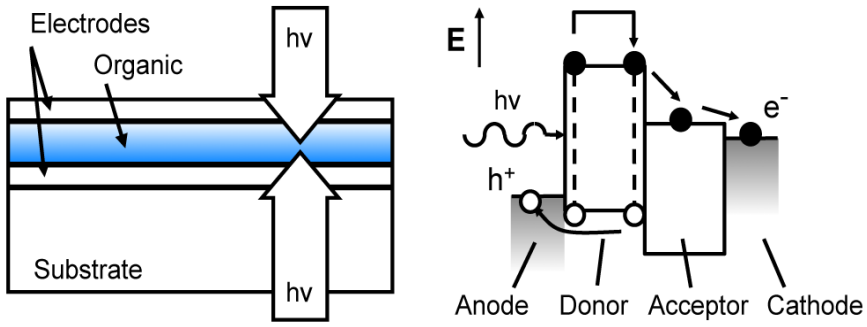

Figure 1-3. A schematic of an organic photovoltaic (OPV) cell structure, similar to that of an OLED. Absorption of photons generates bound excited states (excitons), which upon diffusion to the donor-acceptor interface dissociate into electrons and holes. The light-absorbing layers are often structured to contain partially mixed donor and acceptor components, which are phase separated and crystalline at the nanoscale. [7]

1.2.3. Organic Thin-Film Transistors

Field-effect/thin-film transistors (FETs and TFTs) are the foundational elements of integrated circuits used in computing and information display, where millions of transistors are needed to enable pixel switching across the entire display area. Most transistors are made of single-crystal, polycrystalline, or amorphous silicon. Metal oxides have gained market share recently in display applications; however, OTFTs have attracted considerable attention in the past decade owing to the potential to realize large-area, mechanically flexible, lightweight devices, as well as to reduce the cost of materials and processing over large areas on glass and plastic substrates at room temperature. Over time, organic compounds have been developed with field-effect charge mobilities comparable with or higher than those of amorphous silicon TFTs (e.g., 1–10 cm^2/V-s), enabled by improvements in molecular structure and film morphology control that reduce degra-

dation and act to maximize electronic coupling between the π electron systems of adjacent molecules [34].

Examples of OTFT configurations are shown in **Figure 1-4**; the top-contact/bottom-gate architecture is the most commonly used in research. The source and gate electrodes are biased (V_{DS} & V_G) relative to the drain. The charges, electrons or holes, are injected from the source and accumulate in the organic layer adjacent to the gate dielectric, forming a conducting path. Many organic materials, both small molecular and polymeric, have been used as channel materials for OTFTs [35–37]. Pentacene is one widely explored material, which exhibited a relatively high field-effect hole mobility in the early years of OTFT work. The important metrics used to analyze the performance of OTFTs are field-effect mobility (μ, in cm^2/V-s) of the charge carrier, current On-Off ratio (I_{ON}/I_{OFF}), threshold voltage (V_{TH}, in V), and subthreshold slope (S, in mV/decade) [38], all of which are extracted from the current-voltage characteristics of the OTFT.

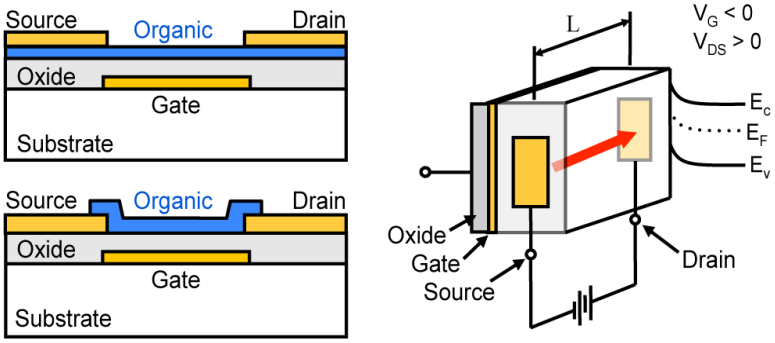

Figure 1-4. A schematic of an organic thin-film transistor (OTFT) with top-electrode and bottom-electrode configurations. On the right is an energy-level diagram showing band bending as a result of applied gate bias, which causes hole or electron accumulation (or depletion) in the region of the semiconductor adjacent to the gate oxide. Bias on the source and drain electrodes causes electrical current (*red arrow*) to flow between source and drain, in the semiconductor region adjacent to the gate oxide. [7]

1.2.4. Other Organic Electronic Devices

Organic semiconductor lasers :

A number of reviews have been published on lasing in organic semiconductors [39–41], although electrically pumped lasing has not been achieved. Optically pumped lasing has steadily gained in efficiency [39]; state-of-the-art distributed feedback polymer lasers operate with lasing thresholds as low as 3.6 W/cm^2, which allows pumping with cheap inorganic diode lasers or even commercially available LEDs. Recent work has exploited the large, two-photon absorption cross-section of polymers to demonstrate nonlinear pumping of a blue-wavelength laser. This may mark a path to the pumping of blue lasers with low-cost red diode lasers to create hybrid, electrically pumped polymer lasers. The replacement of expensive, bulky laser pump sources with small, solid-state diode lasers, which are commercially available and extremely cheap, holds the promise of compact, cheap, organic sources operating at visible wavelengths. Applications, however, still require further reductions in lasing thresholds as well as the demonstration of longer lifetimes and continuous-wave operation before widespread deployment becomes possible.

Organic photodetectors :

Key parameters for photodetectors include efficiency and speed of response. Organic photodetectors based on standard organic materials can sense light in the visible, infrared, and even X-ray portions of the electromagnetic spectrum and can operate well into the megahertz regime [42, 43], with the speed being limited by the size of the device, the lifetime and transport rate of excitons, and the charge carrier mobility. Organic photodetectors are well suited to applications requiring large-area and nonplanar devices, includ-

ing X-ray imagers for biomedical applications [44] and human-eye-mimicking vision systems [45, 46]. Miniaturization of organic photodetectors (e.g., by placing them directly on the cantilever of a near-field scanning microscope [47]) can open new applications in materials characterization and metrology. The low-cost nature of organics also allows them to be used for disposable on-chip sensors [48–50] or data communications, and their chemical tunability allows tunable photo-action spectra to be obtained, which may be useful in colorimetry. [51]

1.3. Thermal properties and purification

1.3.1. Thermophysical properties of organic materials

Small molecular conjugated organic materials exhibit van der Waals bonding in the condensed state, which is stable up to relatively high temperatures (e.g., copper phthalocyanine is stable in air above 350°C). Following the synthesis of the compounds and prior to depositing thin films for devices, the materials are usually purified by using a combination of crystallization precipitation out of solution, column purification, and vacuum-train sublimation. To generate device-quality thin films with precisely controlled thickness (down to <1 nm), the starting materials must be either thermally evaporated or precipitated out of a solvent while process conditions are carefully controlled (e.g., in spin-coating, concentration, temperature, and substrate rotation speed must be controlled). To minimize the incorporation of unintentional stoichiometric/electronic defects during processing, stringent solvent purification and/or vacuum maintenance must be observed. The evaporation temperature window for conjugated polyaromatic compounds (with molecular weight typically ranging between 200 and 1,000 g/mol) is framed by the need to achieve sufficiently high evaporation rates to meet production throughput requirements

and the need to avoid thermal degradation. The evaporation temperature is also set by considerations of desired film morphology—faster deposition rates (and colder substrate) generally lead to amorphous deposits, whereas slower deposition rates (and warmer substrate) generally increase intermolecular ordering in the films [52, 53], which is potentially advantageous in optimizing charge and exciton transport.

To guide the design of deposition apparatus, establish adequate process control, and estimate fundamental limits of production throughput and fabrication energy budget, particularly for commercial-scale fabrication of organic-based devices, evaporation properties of the compounds should be known or predictable. In contrast to traditional hydrocarbons encountered in fossil-fuel refining, the thermodynamic properties of polyaromatic compounds comprising the class of organic semiconductor materials are less well known. Vapor-liquid or vapor-solid equilibrium has been studied by static and kinetic methods (e.g., direct detection of vapor pressure in a closed vessel by a pressure gauge, Knudsen effusion, the Langmuir method, and flow-based techniques [54, 55]), which are applied depending on the range of P_{vap} and evaporation temperature involved. Static methods are simple and reliable but limited to pressures >1 Torr. The Knudsen effusion method is useful for materials with vapor pressure between 10^{-7} and 10^{-1} Torr, at temperatures between 350°C and 600°C, and involves measuring the rate of effusion of equilibrated vapor through a small orifice. For flow-based techniques, accurate and meaningful thermodynamic data can be obtained by using a standard thermobalance [54, 56], which is calibrated with materials of known vapor pressure, with an evaporation rate modeled by the Langmuir equation for free evaporation obeying the classical Clausius-Clapeyron (exponential) dependence on enthalpy and temperature [57].

Shalev & Shtein [56] tabulated thermophysical properties of several archetypal molecules used in organic semiconductor devices, including data reported by others [58–66]. Predictions of the sublimation enthalpy of organic materials can be made via empirically validated group contribution methods [67, 68] and the number of occurrences of different atom types [68]. Shalev & Shtein [56] found a simple relationship between the evaporation enthalpy and crystal density:

$$\Delta H = 163.9 \cdot d - 106.4 \tag{1.2}$$

where ΔH is the sublimation enthalpy (kJ/mol) (typically ranging between 100 and 200 kJ/mol) and d is material density (g/cm^3). (The utility of this relationship is reciprocal: Because the determination of evaporation enthalpy is relatively simple using thermogravimetric analysis, the equation predicts material density in the deposited film.)

1.3.2 Materials Purification

Maintaining high purity of the compounds comprising electronically active layers of devices is essential to obtain the desired performance of the device [69–71]. Impurities may act as deep traps and/or recombination sites within the thin film. Dopants such as oxygen or even water can enter the organic film through unintentional exposure to the ambient, which leads to degradation of the device performance over extended periods of operation [72]. Molecular impurities, such as molecular fractions, that are codeposited with the desired organic semiconductor can disrupt the molecular stacking order, which results in a significant reduction in exciton and charge carrier mobility [71].

Highly conjugated small molecular materials are often poorly soluble in common process solvents and are therefore purified using sublimation techniques, based on the

fact that different molecular solids in general differ in their molecular weight, vapor pressure, and condensation temperature [73, 74]. Train sublimation (or gradient sublimation) [71, 74] is illustrated in **Figure 1-5**; the starting material is heated inside a glass or quartz tube mounted inside a multi-zone furnace that allows close control over the temperature gradient. Because the pressure inside the tube is uniform, evaporation and condensation occur slowly along the tube, such that different molecular moieties separate out according to their evaporation enthalpy, proportional to the specific bonding strength. Since bonding is primarily mediated by van der Waals interactions, a greater number of atoms per moiety (i.e., higher molecular weight) generally correlate with compounds partitioning toward the high-temperature zone, whereas low-temperature impurities with low molecular weight will condense after the purified material, closer to exit from the tube.

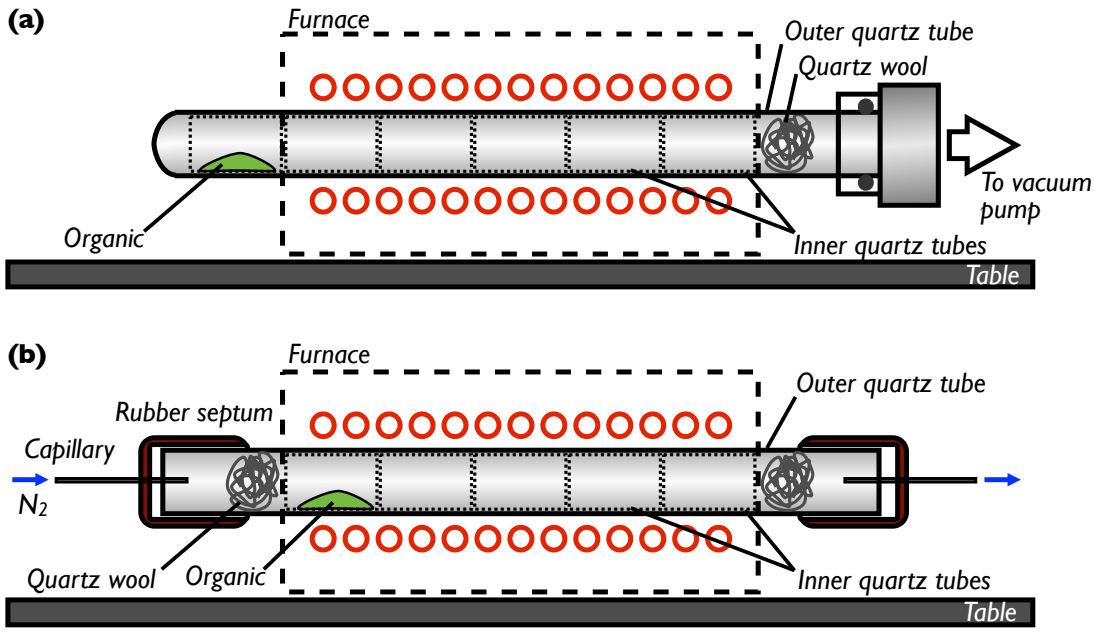

Figure 1-5. Illustration of vacuum train sublimation for material purification.

Fractional impurity concentrations as low as 10^{-4} are achievable by repeating the train sublima- tion procedure [75] multiple times. Note that precise chemical means of measuring impurities in these compounds remain difficult, which necessitates analysis of materials inside devices (e.g., diodes or transistors). Note also that owing to the complex role that impurities play in affecting the properties of the host material, some have observed degradation of device performance beyond a certain level of purity; for example, Rim et al. [76] saw a decrease in solar-cell performance, attributed to reduced band bending at the donor-acceptor heterojunction, because the highly purified PTCBI behaved as an intrinsic semiconductor rather than as the desired *n*-type material.

1.4. Deposition Techniques

As noted above, device performance requirements and fundamental materials properties dictate the deposition methods, which must be capable of producing multilayered thin films, with layer thicknesses defined with subnanometer precision. Degradation of materials must be minimized by processing in an inert environment. Ionization of impurities in organic semiconductor devices is much more limited than in their inorganic analogs, and it can be difficult to ascertain precisely the total concentration of dopants in these materials. The deposition rate should be fast enough to minimize the incorporation of dust and impurities in the growth ambient but slow enough (e.g., <1 nm/s) to allow for precise control over layer thickness and stoichiometry when the layers are doped. (Commercial device fabrication calls for short takt times and consequently may require considerably faster film growth rates than deposition for laboratory-scale research.) OLEDs typically tolerate (and indeed can benefit from) amorphous films, stacked with sharply defined interfaces to help control the injection and recombination of charge, to localize excitons

and facilitate light extraction. Efficient photovoltaic cells have been demonstrated with sharp, blended, and interdigitated interfaces [2, 33, 77–79] that maximize the electron donor-acceptor interfacial area to counteract the typical exciton-diffusion bottleneck in organic materials. The light-absorbing layers in OPV cells also support charge transport and are often processed to achieve nanoscale crystallinity by slow deposition (e.g., <0.1 nm/s) or postdeposition annealing. With the basic considerations outlined above, the most common methods of small molecular thin-film growth are reviewed below.

1.4.1. Organic Molecular Beam Deposition

Organic molecular beam deposition (OMBD), comprehensively reviewed by Forrest [80], was derived from conventional solid-source molecular beam epitaxy, wherein the material to be deposited is placed into Knudsen effusion cells, baked, and subsequently deposited in an ultra-high-vacuum ($<10^{-10}$ Torr) chamber at relatively slow rates (e.g., <0.1 nm/s). The schematic of the OMBD technique is shown in **Fig. 1-6**. The evaporated molecules adsorb onto the substrate through van der Waals forces and can sustain quasi-epitaxial growth for several monolayers, after which strain relaxation results in pronounced stacking defects. The very pure growth environment permits controlled studies of the role of dopants [81], properties of heterogeneous organic-inorganic interfaces [80, 82], interfacial bonding [83–85], and surface energetics [86, 87]. Due to the considerable capital expense and process intricacy, OMBD has remained a relatively specialized technique geared toward fundamental science, where materials purity and interface cleanliness are paramount. A simpler variant, VTE, became more common for device fabrication and material development.

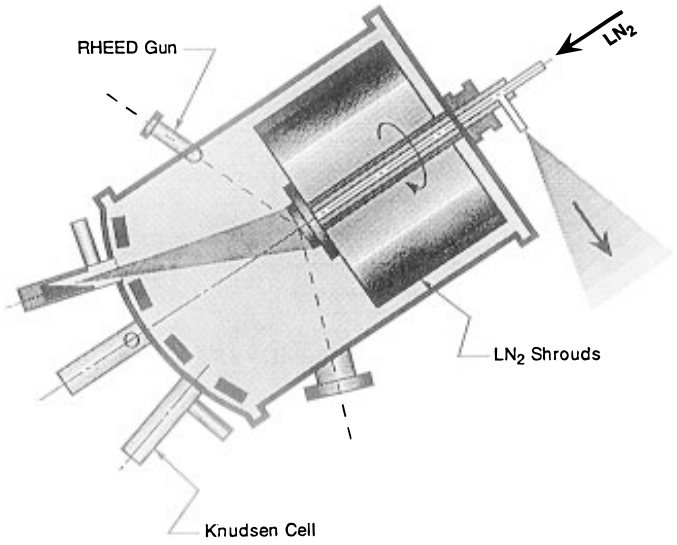

Figure 1-6 Simplified schematic of organic molecular beam deposition apparatus. [80]

1.4.2. Vacuum Thermal Evaporation

VTE is similar to OMBD but relaxes the vacuum requirements to ~10^{-7} Torr, where the molecular mean free path, λ, is on the order of 100 m (modulated by the size of the evaporant molecule). Resistively heated evaporation containers are used (**Figure 1-7**), which permits the deposition of organic compounds, nonrefractory metals, and some inorganic compounds in a line-of-sight fashion. The film deposition rate, r_{dep}, is linear with the source material vaporization (sublimation) rate, r_v, which itself is exponential with temperature:

$$r_{dep} = \eta_{mu} \cdot r_v = \eta_{mu} \cdot A \cdot exp(-\Delta H^{vap} / R \cdot T) \tag{1.3}$$

where η_{mu} is the material utilization efficiency, A is a material- and apparatus-specific coefficient, ΔH^{vap} is the vaporization enthalpy, R is the ideal gas constant, and T is the

source-material temperature. In the simplest case of a noncollimated, point-like evaporation source, film deposition rate, and hence the deposited film thickness, at any point on the substrate has a cosine squared shape:

$$h = h_0 \cdot \cos^2 \theta \tag{1.4}$$

as illustrated in **Figure 1-7**.

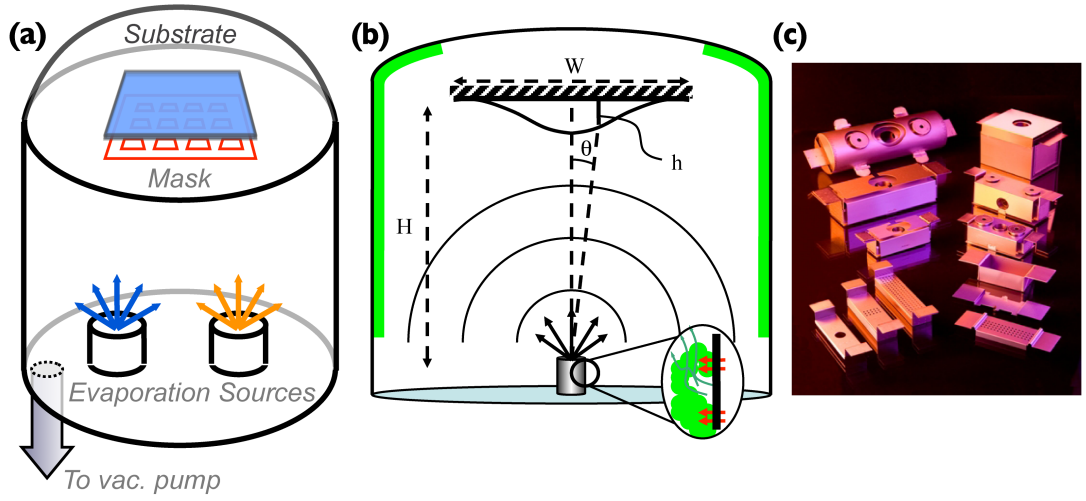

Figure 1-7 Vacuum thermal evaporation: (*a*) A simplified schematic of a vacuum thermal evaporation (VTE) chamber, shown with two sources and a shadow mask. Co-evaporation of the materials permits doping with reliable control over stoichiometry down to 0.1% concentration levels. (*b*) An illustration of film nonuniformity inherent in point-source deposition, as well as unevenness of heating inside the evaporation source due to the poor thermal conductivity of crystalline organic powders. (*c*) Typical evaporation containers used in VTE. Note that industrial applications typically entail larger, linear or multiple point-sources designed to achieve uniform deposition of >1-m-wide substrates. [7]

Thus, to achieve a thickness variation smaller than a fraction f over a span of substrate b, the throw (distance from source to substrate) H should be $H \geq b/f$. Practically, longer

throws result in substantially increased pumping requirements (because chamber volume scales roughly as H^3), while leaks and outflaming scale as H^m with $1 \leq m \leq 2$. To mitigate the obvious trade-off between thickness uniformity and pumping costs, one can arrange a series of point sources (**Figure 1-7*c***) such that the $\cos^2\theta$ profiles from each one overlap, leading to a flatter deposit. From **Equation 1.3**, it is also clear that achieving tight control over dopant concentration in VTE requires very close control over the evaporation source temperature, because a minute deviation in temperature from set-point of either of the sources can result in a large swing in the deposition rate and, hence, the deposited host-to-dopant ratio.

As indicated in **Figure 1-7*b*** (*inset*), non-uniform packing of the source material in the evaporation container can lead to fluctuations in the evaporation rate. The thermal conductivity of purified organic powder is low [88, 89], such that evaporation is fastest at the hot container wall. Non-uniform heat and material distribution work to create empty pockets that collapse and can potentially perturb the evaporation rate. Finally, to accelerate deposition, source temperature must be in- creased; however, for a given source-to-substrate area ratio, an intrinsic limit to the deposition rate arises due to the limited thermal stability of the organic compounds (typically, <500°C).

1.4.3. Organic Vapor Phase Deposition

OVPD was developed to address some of the limitations of VTE. Based on hydride vapor phase epitaxy, OVPD proceeds by thermally evaporating source material into a carrier gas that transports it toward a cooled substrate, where the organic material selectively condenses. With appropriate temperature and flow profiles [62], material utiliza-

tion efficiency can exceed 40% - orders of magnitude greater than that for typical VTE, especially in laboratory-scale apparatus. Two in- depth studies of the transport mechanisms governing OVPD have been published [62, 90]; here, a brief discussion suffices to contextualize the additive patterning methods of OVJP and GF-OVJP.

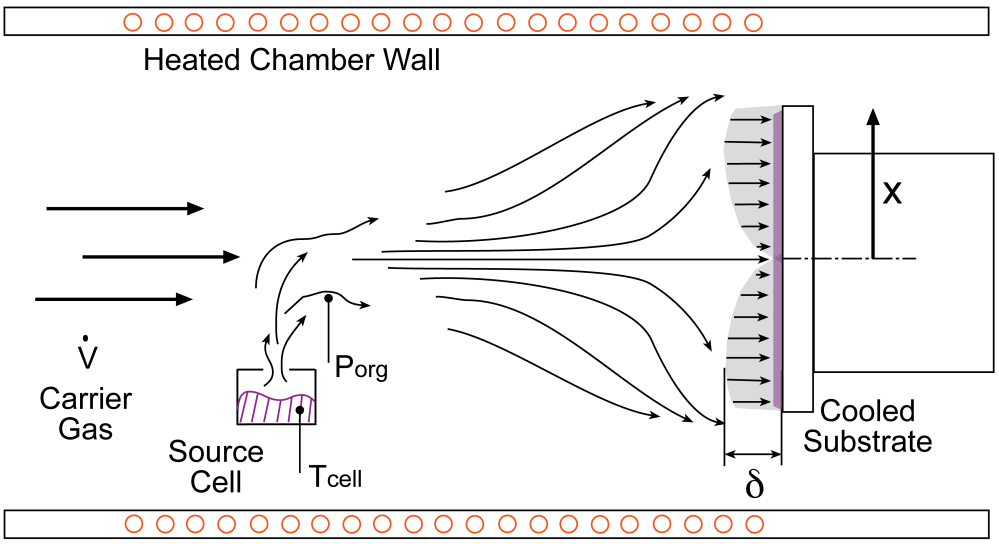

Figure 1-8. An illustration of organic vapor phase deposition (OVPD), where organic source material is evaporated into a stream of hot carrier gas. The vapor and carrier gas flow toward a cooled substrate, where selective condensation of organic material occurs. Flow and boundary-layer uniformity contribute to growth of films of uniform thickness across the substrate; δ denotes the boundary-layer thickness. [62]

By separating the evaporation, transport, and deposition processes in space (**Figure 1-8**), OVPD improves control over the deposition rate and coating uniformity. The rate at which organic vapor is extracted from the source is proportional to the vapor pressure, which is still exponential with temperature via the Clausius-Clapeyron equation. Howev-

er, a self-contained evaporation source can comprise a larger thermal mass and allows for the grouping of several materials with similar vapor pressures into fewer heating zones or furnaces, whereas the hot carrier gas can flow through the packed bed of organic source material - factors that minimize spatial and temporal temperature fluctuations within the organic powder. Make-up flow can be used to dilute the vapor as needed; to reduce counter-diffusion of organic molecules upstream, toward the sources; and to help shape the distribution of the material over the substrate. Maintaining the flow path and deposition chamber at temperatures above the condensation point of the organic material nearly eliminates parasitic condensation on the deposition chamber walls, which dramatically improves apparatus cleanliness and reduces downtime for cleaning. Reduced material buildup on the chamber walls and continuous flow of carrier gas help reduce dust accumulation on the substrate.

Typical operating temperatures range from 200° C to 500° C, mass flow rates are 10–1,000 sccm, and pressures are in the range of 0.1–10 Torr (corresponding to $100 < \lambda < 1$ μm). Continuum- based (i.e., Navier-Stokes) models of transport are valid [62], except for patterning, as discussed later. The low pressure limit arises from the need to generate sufficient flux of carrier gas molecules to transport organic vapor at a rate that overcomes transport by random diffusion and thermal convection (i.e., to ensure Péclet numbers >10), and the high limit arises from the need to maintain sufficiently low pressures near the substrate to maximize diffusion-limited condensation. Typical Reynolds numbers are <100, well below the turbulent threshold, although momentum transfer due to free diffusion between flow lamina can be substantial. Carrier flow around the cooled substrate gives rise to hydrodynamic and thermal boundary layers. The cold-substrate boundary

condition means that organic vapor concentration falls to zero near the substrate surface, which gives rise to a concentration boundary layer as well. Film deposition occurs by diffusion of material across this boundary layer. The flow pattern can be engineered to achieve uniform distribution of the vapor above the substrate, in turn achieving uniform film thickness. In this fashion, film thickness uniformity is decoupled from the geometry of the source. Analysis of the physical processes governing evaporation, transport, and deposition shows that the net rate of film deposition can be expressed by

$$\frac{r_{dep,i}}{A_{sub}} = j_i = \eta_{dep} \cdot \frac{D_i}{\delta} \frac{P_{0,i} \exp\left(\frac{-\Delta H_i^{vap}}{RT_{cell}}\right)}{\left(\frac{\sqrt{2\pi \cdot mw_i \cdot RT_{cell,i}}}{\alpha_i \cdot A_{org,i}} + \frac{RT_{std}}{\dot{V}_{i,sccm}} \times \frac{P_{cell,i}}{P_{std}}\right) \times \left(\sum \dot{V}_i + \dot{V}_{dil}\right)} \tag{1.5}$$

where $r_{dep,i}$ is the deposition rate (usually expressed in units of film thickness per unit time); A_{sub} is the substrate area; and η_{dep} is the deposition efficiency, which depends on the gas distributor design and the resulting flow pattern around the substrate. The variables (indexed by each component, i, being deposited) are as follows: η_{dep} is deposition efficiency (subject to the flow pattern and apparatus geometry), D_i is organic vapor diffusivity of molecule i in the carrier gas, δ is boundary-layer thickness, $P_{0,i} \exp\left(\frac{-\Delta H_i^{vap}}{RT_{cell}}\right)$ is equilibrium organic vapor pressure, mw_i is molecular weight of i, T_{cell} is evaporation cell temperature, $A_{org,i}$ is surface area of the evaporating material i, T_{std} is standard temperature, R is universal gas constant, $V_{i,sccm}$ is volumetric flowrate in sccm of the carrier gas, V_{dil} is volumetric flow rate of the diluting make-up flow, $P_{cell,i}$ is the total pressure inside the evaporation cell of component i, and P_{std} is standard pressure. To predict the deposi-

tion rate for a given reactor geometry, the flow equations must be solved to provide information about δ, whereas more precise values for D_i can be either obtained experimentally or estimated from correlations such as the Chapman-Enskog equation [91–93]. The relationship between process parameters and deposition rate embodied by **Eq. 1.5** was shown experimentally to be valid [94] and also forms the foundation for OVJP, described later. Note also that flash evaporation [95] and related methods [96] have been demonstrated. In these techniques, the material to be deposited is fed into a flash evaporation chamber, where solid-to-vapor conversion is nearly instantaneous. The vapor exits the elongated evaporation chamber in the form of a uniform sheet of material directed at a substrate moving perpendicular to the flux. Kodak claimed material utilization efficiency in excess of 50%, although this number is likely to be reduced substantially when patterning (by shadow masking) is taken into account [97].

1.4.4. Controlling Morphology via Process Conditions

Crystallinity and molecular orientation of organic films strongly influence charge mobility. For instance, increased molecular order can result in better charge mobility and improved exciton-diffusion efficiency [98, 99]. However, use of amorphous films at the donor-acceptor interface in OPVs decreases the interaction between donor and acceptor molecules and minimizes the parasitic polaron-pair recombination rate [99]. Morphology of deposited films can also affect the total junction area as well as contact continuity. All these factors must be taken into account when choosing a deposition technique. During film formation, the driving forces that induce nucleation, growth, and crystallization of organic semiconductors strongly depend on the kinetic and thermal properties of the arriving admolecules. In VTE, for instance, the molecular motion is ballistic with relatively

high kinetic and low thermal energies; therefore, the film is usually smooth with an amorphous structure. Note that increasing substrate temperature to promote crystallization can dramatically lower the sticking coefficient. In contrast to VTE, in OVPD the spatially averaged molecular kinetic energy is low due to randomizing collisions, whereas the thermal energy imparted to the topmost layers of the film is high as a result of the much larger frequency of carrier gas molecule collisions with the substrate. Furthermore, a blanket of carrier gas above the substrate can redirect desorbing molecules back toward the substrate. As a result, polycrystalline films can be more readily obtained [100, 101] for a given rate of deposition that would result in amorphous films by VTE. In OVJP, molecular velocity and temperature can be adjusted, and therefore molecular orientation and morphology can be controlled more closely. For example, when films are deposited by GF-OVJP, guard flow effects crystallinity, morphology, and device performance in OPV devices, and Kang *et al*. [102] showed how carrier gas temperature effects pentacene thin-film formation in OTFTs.

1.5. Patterning of organic devices

The above descriptions of VTE and OVPD assume that the objective is uniform deposition of thin films over the entire substrate area. Both techniques allow for nanometer-scale control over film thickness, although OVPD generally offers better control over film composition. Commercial production of devices most often requires the in-plane patterning of electronically active features, which is an essential consideration in the development of organic thin-film deposition technology. Because organic semiconductors are typically van der Waals bonded in the thin films, they are not easily amenable to conventional photolithography-based film patterning approaches.

1.5.1. Vacuum Thermal Evaporation and Shadow Masking

In conventional VTE, organic thin films are typically patterned by depositing through a shadow mask, a thin stencil placed in (near) contact with the substrate during deposition. For a mask aperture with straight walls and thickness, t, and using a source of width, l, centered on the aperture axis, the shape of the deposit is approximately trapezoidal, with the width of the edge taper and, hence, the resolution limit, ρ, approximated by

$$\rho \approx (s + 2t)l / 2h \tag{1.6}$$

Here, s is the mask-substrate separation, and h is the source-to-mask distance, as defined in **Figure 1-9**.

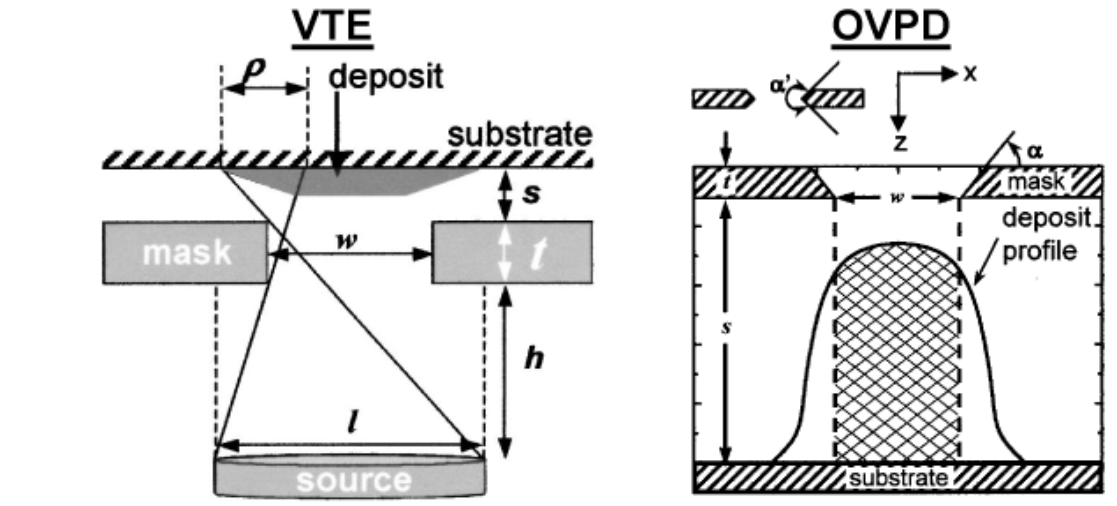

Figure 1-9. Schematic of pattern formation by shadow masking in vacuum thermal evaporation (VTE) (left) and OVPD (right). The deposit shapes are slightly different for the two methods; VTE typically results in trapezoidal profiles, and OVPD yields bell-shaped profiles, due to molecular collisions in the vapor phase above the substrate and in the aperture gap. [106]

The design guidelines suggested by **Eq. 1.6** are intuitive: The mask should be as thin as possible, and *s* should be small, to produce the sharpest edges. However, the mask also should not bow under its own weight, and it should withstand multiple mount-remount and cleaning cycles. Thus, practical mask dimensions represent a compromise between the pattern resolution and hardware robustness requirements, with typical values for *s*, *t*, and aperture width of approximately 10 μm, 70 μm, and 100 μm, respectively. In research-laboratory-scale apparatus, the typical source diameter is $l \approx 1$ cm, and source-to-substrate distance is $h \approx 50$ cm, which yields $\rho \approx 2$ μm, which is adequate for full-color OLED displays. Note, however, that dimensional run- out owing to thermal expansion is a critical consideration for large-area patterning. The aperture profile can be designed with a bevel or double lip, such that the edge is thin despite the rest of the mask being thick for mechanical robustness, as shown in **Figure 1-9**. In some instances, it may be advantageous to integrate the mask with the substrate, as demonstrated by several researchers [103, 104], or even to exploit the parallax owing to the gap between mask and substrate to control the placement of the evaporated components [105].

1.5.2. Organic Vapor Phase Deposition and Shadow Masking

Shtein *et al*. [106] studied shadow masking in combination with OVPD to pattern active organic layers. Depending on the process pressure, the molecular mean free path can be short enough (i.e., 1–1,000 micrometers) to cause numerous collisions in the vicinity of the mask and, indeed, in the space between the mask and the substrate. In this regime, where the Knudsen number (*Kn*) is $0.1 < Kn < 10$, the edge dispersion of the patterned deposit is expected to be larger and of a different shape than that in VTE, and the walls of the aperture itself are expected to be coated as well, as shown in **Figure 1-9**. Defining a

pixel shape factor as the ratio of aperture width, *w*, to the total deposit width, Shtein *et al*. [106] studied the effects of deposition pressure, mask-substrate separation, mask thickness, and aperture shape on pattern resolution. The best shape factors were seen for tapered apertures (narrowest near the substrate) that were in contact with the substrate. Higher pressures resulted in more diffuse pattern edges, as well as more parasitic coating of the aperture walls.

To address the issue of parasitic coating of the mask walls, the mask can be heated [106], but as noted above, simple heating of the mask could result in undesired transfer of heat to the substrate, which could potentially reduce the molecular sticking coefficient or evaporate the deposited layers. Instead of relying on diffusion through apertures to form the patterns, vapor jets could be used [106, 10]. The method of OVJP for efficient, rapid, additive patterning of organic active and passive layers is discussed below in Organic Vapor Jet Printing.

1.5.3. Molecular Jet Printing

Integration of the shadow mask with the evaporation sources has been shown in the form of molecular jet printing (MoJet), which enables direct evaporative patterning of low-molecular- weight organics and metals at high resolution [107]. In principle, the technique combines the advantages of the film purity of thermally evaporated films with the speed of direct patterning, leveraging the precision and scalability of microelectromechanical system (MEMS) technology for the actively controlled apertures. Deposition of active organic devices (e.g., OLEDs and OFETs) has been shown with pattern definition on the order of 5 μm [108]. A MoJet printing system is schematically shown in **Fig. 1-10**.

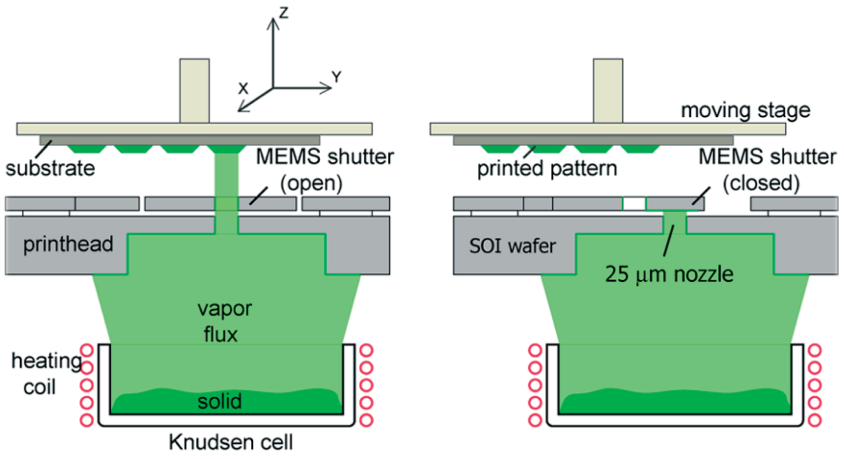

Figure 1-10. Illustration of the molecular jet printing apparatus and process. [108]

The entire printing system is housed inside a vacuum chamber at a base pressure of 10^{-7} Torr, with the substrate mounted on a precision motion stage above the printhead. The printhead is composed of a membrane aperture (nozzle) and an integrated comb-drive-actuated microshutter, which modulates the flux of evaporated materials through the nozzle [107]. The Knudsen cell is used to generate evaporated material flux from underneath the print- head. The materials to be deposited are loaded in an aluminum or quartz crucible and heated above the sublimation/boiling temperatures. The printing system operates as a single-nozzle printer. The technique is reconfigurable for digital fabrication of arbitrary patterns with multiple material sets and is potentially scalable to coating large area substrates. The printed pixel size and profile are strongly dependent on the geometry of the printer system and follow geometric considerations similar to those of shadow masking in VTE [108, 109], with pattern resolution given by

$$\rho \approx (s+t)(D-w)/2h + s(D+w)/[2(h+t)] \tag{1.7}$$

Courcimault & Allen [110] reported a microelectromechanical system (MEMS)-based masking system, integrated with the substrate for submicrometer patterning of metal contacts, which achieved patterning, for example, of metal lines 1.1 μm by 10 μm, spaced by 0.3 μm. They also reported a self-aligned masking configuration in which a sequence of processing steps (photoresist + mobile mask + laser ablation) resulted in a tapered mask directly on the substrate. Deposition of metal through this mask, followed by liftoff, can result in a high-resolution patterned metal contact. This approach, however, is likely suboptimal for patterning active organic films, or even metal contacts directly onto the organic film, because liftoff requires the use of a solvent bath that could dissolve the organic layers.

A desirable feature of MoJet is the ability to additively pattern high-melting-temperature metals to form contacts. However, the MEMS printhead is hot, requiring baffles that can reduce material utilization efficiency, and is susceptible to clogging after prolonged use due to accumulation of a thick film of material on the backside of the shutter and aperture.

1.5.4. Inkjet Printing and Laser-Induced Thermal Imaging

Processing of polymer-based organic semiconductors most often entails the use of solvents, because the polymeric semiconductors are typically more soluble than small molecular semiconductors in common process solvents. Traditionally, uniform application across the entire substrate by spin-on or spray-on methods was employed, but it required additional and relatively costly steps to pattern electronically active layers. This shortcoming was addressed by inkjet printing [111, 112]. Note, however, that due to droplet drying energetics and dynamics, microscale features must be prepatterned on the

substrate to generate individual wells that maintain a flat pixel profile upon drying [113, 114]. Commercial use of inkjet printing has so far been successful in depositing transistor channels, and to a more limited extent OLEDs, in part due to the efficiency limitations of polymeric emitters relative to the small molecular electrophosphorescent and fluorescent compounds.

Additional methods for active-layer patterning include a variety of stamping/transfer techniques [115–119] and LITI [120] (**Figure 1-11**). In LITI, a donor substrate is first coated with the material to be deposited. The donor substrate is then brought into physical contact with the receiver substrate and is illuminated by a short, powerful laser pulse from the back, which causes the transfer of material. High-resolution OLEDs and OTFTs have been made by using this technique [121].

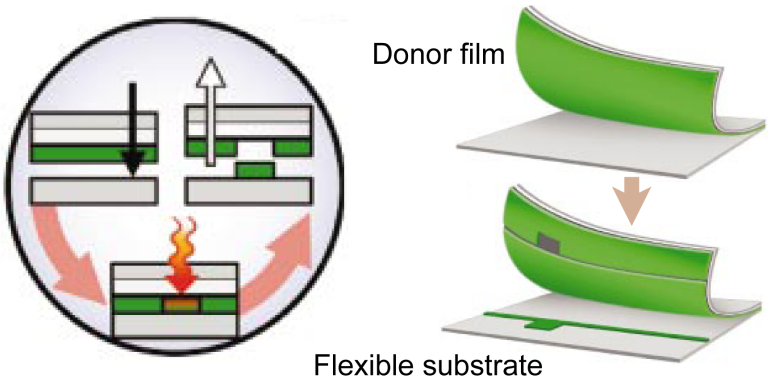

Figure 1-11. LITI: A schematic of the laser-induced thermal imaging process, where active organic films are desorbed from the donor sheet and transferred onto the receiver substrate by a laser pulse. [120]

Advantages of LITI include its applicability to a broad spectrum of organic materials, patterning accuracy (±2–5 μm compared with ±15–20 μm for shadow-masking and inkjet-printing techniques), ability to pattern multilayer structures in a single step, scalability of the process to large substrates, and ability to reach production-scale takt time requirements [122]. However, LITI introduces thermal defects in the organics materials during patterning due to the ablation process. The process is extremely sensitive to particulates and similar contamination of substrate and donor surfaces, which places stringent requirements on processing-atmosphere cleanliness. Furthermore, LITI requires a primary deposition process to create the (multilayered) films on the donor substrate in the first place, which potentially adds cost and complexity. Material transfer from a donor stamp prepatterned with a relief structure can be useful (provided the stamp can be cleaned and reused) and potentially mitigates the thermal damage but remains sensitive to particulate contamination.

1.6. Organic Vapor Jet Printing

To address the limitations of shadow masking in combination with VTE or OVPD, and to enable direct, additive patterning for small molecular organic semiconductors, a new technique was developed in the early 2000s: OVJP [9]. As illustrated in **Figure 1-12**, similar to the process in OVPD, the organic material is evaporated into a carrier gas, which, upon picking up the vapor, is ejected at high velocity through a collimating nozzle directed at the cooled substrate.

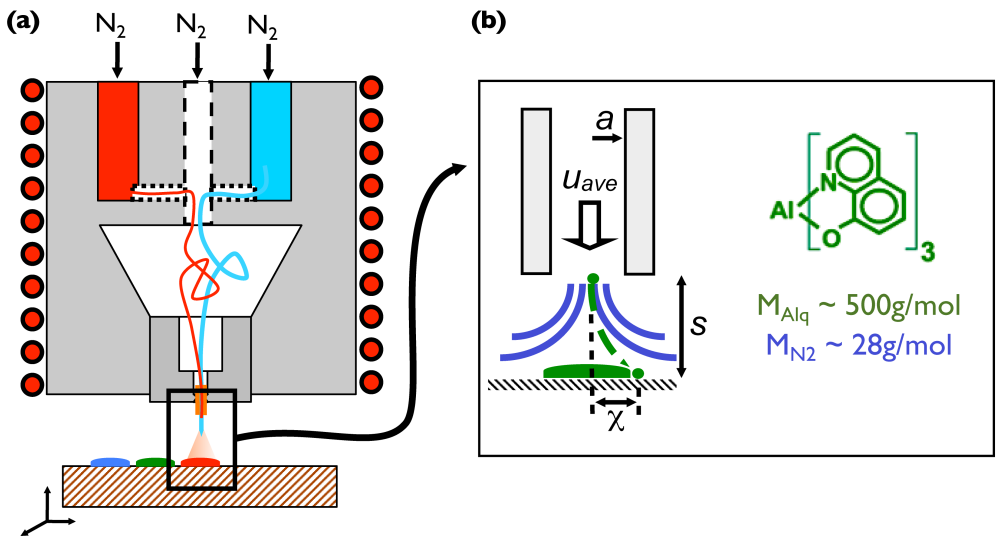

Figure 1-12. Organics vapor jet printing: **(***a***)** Schematic of the organic vapor jet printing (OVJP) apparatus, shown with two source cells, a center dilution channel, and a modular collimating nozzle, all heated from the outside. A hot inert carrier gas enters the apparatus, picks up the organic vapor, and ejects the gas mixture through the nozzle. The collimated vapor jet impinges onto a cooled substrate where the organic molecules selectively physisorb, forming a well-defined deposit. **(***b***)** Diagram defining the geometry relevant to pattern formation, also depicting the diverging carrier gas (N_2) flow streamlines and the collimated trajectories of heavier organic molecules. [124]

Mass conservation principles suggest that the master equation (**Equation 1.5**) developed for OVPD should still hold true in describing the net rate of material delivery via the nozzle in OVJP, with the main difference being the pressure inside the evaporation cell and the gas (fluid) dynamics in the region between the nozzle and the substrate. A pressure drop is required across the nozzle to achieve flow collimation, which implies that the net gas overpressure experienced by the organic material in the source cell is generally larger than that in OVPD. Consequently, the effective vapor pressure of the organic material is lowered, which requires the source temperature or total evaporative area

to be increased to compensate for the drop in effective vapor pressure. (Note that the drop in vapor pressure is roughly linear with overpressure, whereas net evaporation rate is exponential with temperature.)

After the organic vapor is entrained in the carrier gas being driven through the collimating nozzle, the jet rapidly expands due to a combination of pressure drop and proximity of the substrate. The carrier gas does not condense on the substrate, flowing outward from the axis of the nozzle at a rate that is inversely proportional to the nozzle-to-substrate distance. Owing to the symmetry of the apparatus, flow in the region directly downstream of the nozzle and above the substrate is stagnant, with a boundary layer that can have a nontrivial dependence on process variables. Transport of organic molecules across this stagnation zone determines the printed feature size, deposition rate, and material utilization efficiency. As **Figure 1-12** illustrates, the organic molecules have a mass lower than that of the carrier gas and thus follow trajectories different from those of the latter, determined by the temperature, pressure, and geometry of the apparatus.

Typical downstream vacuum levels on the order of 0.1–10 Torr (similar to those in OVPD, achieved using cost-effective roughing pumps) are sufficient to reduce λ to the 10–100 μm range, although the dynamic pressure in the region between the nozzle and the substrate can easily exceed 10 Torr. Nevertheless, λ can fall within an order of magnitude of critical apparatus dimensions—namely, nozzle diameter and nozzle-to-substrate separation distance—and operation within this intermediate regime (i.e., where the *Kn* ranges between 0.1 and 10) can complicate process modeling.

A simple scaling analysis reveals how patterning resolution depends on the major process variables. The analysis assumes that organic molecular dispersion is driven prin-

cipally by isotropic diffusion and by the outward flow of the carrier gas. Because of the heterogeneous and partially molecular nature of the flow in the deposition region, the number of molecular collisions and the mass differential between the carrier gas and organic molecules provide a rough guide to the net amount of sideways deflection an organic molecule will experience during its transit from the nozzle exit toward the substrate:

$$\chi / a \approx (s / \lambda)(m_{cg} / m_{org}) + [D \cdot s / (u_{ave} \cdot a^2)]^{1/2} \qquad (1.8)$$

where χ is pattern dispersion, a is nozzle diameter, s is nozzle-substrate separation, λ is molecular mean free path at the working pressure, m_{cg} and m_{org} are the carrier gas and organic molecular weights, D is organic molecular diffusivity in the carrier gas at the working pressure, and u_{ave} is average flow velocity through the nozzle. The left-hand side of the equation is a scaled amount of pattern dispersion, the first term on the right-hand side of the equation denotes the scaled amount of deflection experienced by the organic molecules via the outflowing carrier gas, and the second term on the right-hand side denotes the contribution of isotropic molecular diffusion. Experiments that vary s, m_{cg}, and λ via the chamber pressure confirm the trend predicted by **Equation 1.8**. Moreover, direct-simulation Monte Carlo models [10, 123, 124] that track molecular trajectories and deposit shapes confirm these predictions. (Note also that the material utilization efficiency, in the absence of secondary flows, surface features, or exhaust manifolds, will follow a trend that is complementary to pattern dispersion. That is, greater pattern dispersion denotes a decreasing net material utilization efficiency.)

Shtein *et al*. [10, 124] initially demonstrated the OVJP process by using single glass capillaries and also single 20-μm-diameter, laser-drilled, stainless-steel nozzles to print patterns of neat organic material. Feature sizes of 30 μm were obtained, which translated to printing resolutions of over 500 dots per inch. An example of a printed pattern and the system geometry are shown in **Figure 1-12**. The OVJP tool was used to draw continuous films of pentacene and make organic TFTs with hole mobilities of 0.2 cm^2/V-s, comparable with those achieved by VTE-grown films [9]. Fluorescent emission α-NPD-Alq_3 OLEDs with EQE = 0.84% were also grown by this method. The efficiency of the fluorescent OLEDs grown by OVJP was comparable with that of conventionally processed devices [124]. Very high local deposition rates (e.g., well over 100 nm/s) were achieved. Subsequent work by Arnold, McGraw, and colleagues [126, 127] showed that high-efficiency, doped electrophosphorescent OLEDs can be realized by OVJP on a common substrate by using a MEMS-fabricated multinozzle array. In-plane patterning resolution on the order of a micrometer has been shown [128]. Furthermore, the overall material utilization efficiency, particularly in laboratory-scale apparatus, is found to be orders of magnitude greater than that in VTE or OVPD. These capabilities in principle enable the use of OVJP for both non- patterned and patterned film deposition over a wide range of applications and production volumes.

As mentioned previously, the ability to create discrete patterns is often required in the fabrication of organic devices (e.g., in typical subpixel layouts in the emissive components or backplane electronics for OLED displays). To enable pixilation of the deposit at high deposition rates, Yun and coworkers [129] developed digital-mode OVJP, wherein the vapor jet can be vented through a digitally controlled valve (**Fig. 1-13**) before reaching the nozzle exit.

Note, however, that when applying the same OVJP process to deposit in the atmosphere, a significant limitation arises: The hot organic vapor mixes with the surrounding oxygen and moisture en route to the substrate. Because the highly conjugated organic semiconductor compounds are susceptible to oxidative damage at elevated temperatures, their device-relevant properties (e.g., luminescence efficiency) usually degrade in air, which lowers device performance.

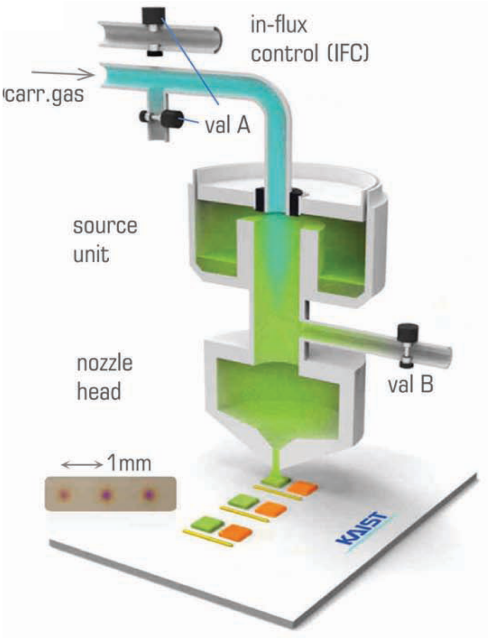

Figure 1-13. Schematic of a digital-mode organic vapor jet printing (D-OVJP). [129]

1.7. Guard Flow-enhanced Organic Vapor Jet Printing

In order to deposit and pattern device-quality organic thin films in air, a guard flow is added to OVJP set up. When depositing at ambient conditions, the downstream pressure is 1 bar, and the hot organic vapor can mix with the surrounding oxygen and moisture en route to the substrate, potentially causing oxidation at elevated temperatures and compromising device performance. Degradation is mitigated by concentrically surrounding the primary jet with a secondary jet of inert gas. The experimental apparatus shown in **Figure 1-14** consists of two glass tubes pulled to form a coaxial nozzle with the inner tube diameter of ~ 200 μm (d_{CG}) and an annular gap of ~100 μm (d_{GF}). The evaporant organic powder is placed inside the inner tube and heated above the sublimation temperature (T_{Source}) of the compounds at the upstream pressure ($P0$), and the nozzle walls were maintained at a temperature higher than T_{Source} to prevent parasitic condensation. The nozzle-substrate separation (s) in the initial GF-OVJP experiments was maintained between 0.5 – 1 mm, while the substrate was mounted on a three-axis linear motion stage, with the substrate holder chilled to maintain its temperature below 40◦C ($T_{Substrate}$) in the ambient. Because the mole fraction of organic molecules entrained in the jet is less than 10^{-3} in all of these experiments, the thermal conductivity (κ) and viscosity (μ) for both the primary and guard jet can be approximated by those of the carrier gas. The carrier gas flow rate (Q_{CG}) of the main jet and the guard jet mass- flow rate (Q_{GF}) were controlled by using mass-flow controllers. The process therefore entailed more than six independently controllable parameters, Q_{CG}, Q_{GF}, T_{Source}, $T_{Substrate}$, translation speed of the substrate (v_x), and nozzle geometry (d and d_{GF}), apart from the choice of inert gas used for the carrier gas and guard flow—considerably more parameters than those used in

VTE or OVPD. This wider choice of process parameters potentially enables access to a wider range of deposition regimes, which in turn enables formation of films with new morphologies that are not easily accessible by using traditional growth techniques. [11, 130, 131]

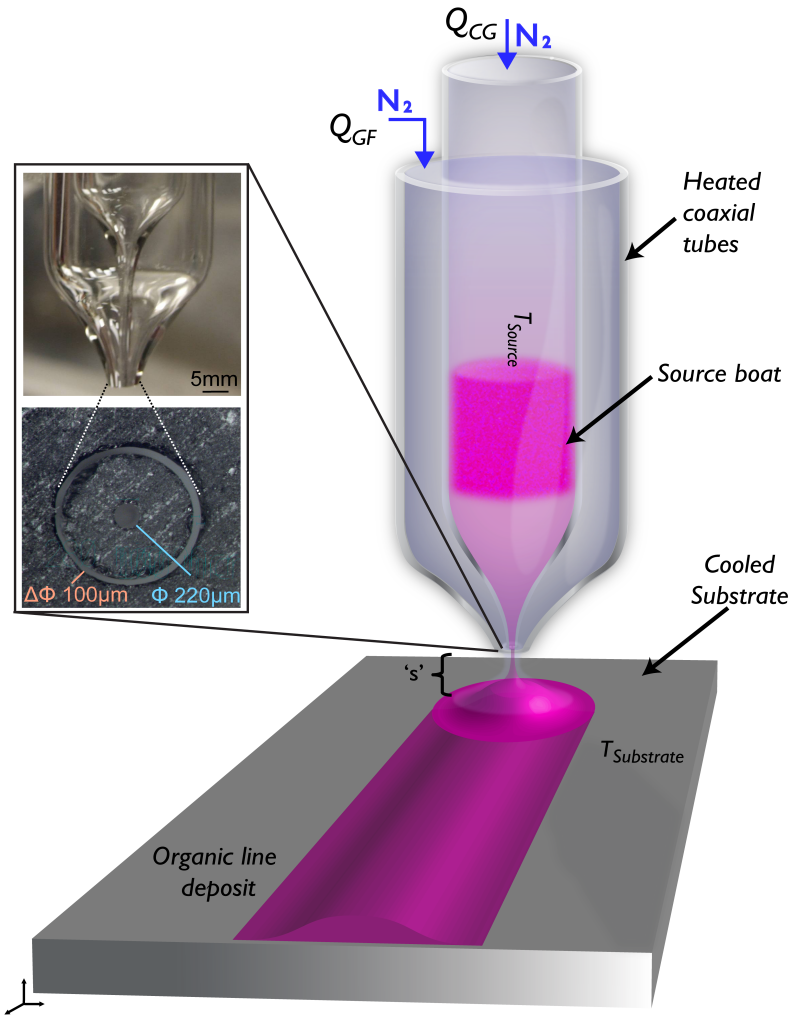

Figure 1-14 Schematic of the GF-OVJP dual-nozzle apparatus, along with the independently controllable process parameters. The nozzle provides for an annular inert guard jet to shield and hydrodynamically focus the organic vapor-containing primary jet when printing in air. The inset shows the side view and cross-section images of the nozzle. [131]

1.8. Summary

Since the early discoveries of photovoltaic effects and electroluminescence in conjugated organic compounds and the pioneering work of Tang on heterojunctions, the performance of organic semiconductor materials and device architectures has steadily improved. Small molecular com- pounds comprise a large fraction of commercially viable materials at the heart of the devices in question (e.g., organic LEDs, solar cells, transistors, sensors). They are generally incompatible with processing approaches deployed in traditional microelectronic manufacturing. Consequently, there is considerable room (and, indeed, urgency) to develop scalable deposition and patterning methods for this class of materials.

The success of commercial-scale, organic-based optoelectronics is contingent upon the ability to scale up thin-film deposition methods to large (e.g., >4 m^2) substrates and the ability to achieve rapid deposition and patterning with fine control over pixel dimensions (e.g., < ±1 nm in thickness and < ±5 μm). Future development is anticipated to also include refinement of additive patterning capabilities, improvements in deposition speed and morphology control, and minimization of the energy budget for processing. GF-OVJP is a technique that enables mask-free, solvent-free, direct, additive patterning and deposition of small molecular materials in air, with potential for control of morphology and electronic properties via the processing parameters.

1.9. References

[1] D. Kearns, M. Calvin, "Photovoltaic effect and photoconductivity in laminated organic systems", *J. Chem. Phys.* **1958**, *29*, 950.

[2] C. W. Tang, "Two-layer organic photovoltaic cell", *Appl. Phys. Lett.* **1986**, *48*,183.

[3] Y. K. Soo, L. J. Yeob, "Organic materials for deep blue phosphorescent organic light-emitting diodes", *Adv. Mater.* **2012**, *24*, 3169.

[4] B. W. D'Andrade, J. Esler, C. Lin, V. Adamovich, S. Xia, et al.,. "Realizing white phosphorescent 100 lm/W OLED efficacy", *Proc. SPIE Org. Light-Emit. Mater. Devices XII,* **2008**, *,* 7051.

[5] M. A. Green, K. Emery, Y. Hishikawa, W. Warta, E. D. Dunlop, "Solar cell efficiency tables", *Prog. Photovoltaics: Res. Appl.* **2012**, *20*, 12.

[6] J. Smith, W. Zhang, R. Sougrat, K. Zhao, R. Li, et al. "Solution-processed small molecule-polymer blend organic thin-film transistors with hole mobility greater than 5 cm^2/V^s", *Adv. Mater.* **2012**, *24(18),* 2441.

[7] S. Biswas, O. Shalev, M. Shtein, "Thin-Film Growth and Patterning Techniques for Small Molecular Organic Compounds used in Optoelectronic Device Applications", *Annu. Rev. Chem. Biomol. Eng.* **2013**, *4*, 289.

[8] J. N. Israelachvili, *Intermolecular and Surface Forces*, Burlington, MA: Academic. **2011,** pp 107.

[9] S. R. Forrest, "Ultrathin organic films grown by organic molecular beam deposition and related techniques", *Chem. Rev.* **1997**, *97*, 1793.

[10] M. Shtein, P. Peumans, J. B. Benziger, S. R. Forrest, "Direct, mask- and solvent-free printing of molecular organic semiconductors", *Adv. Mater.* **2004**, *16*, 1615.

[11] S. Biswas, K. P. Pipe, M. Shtein, "Solvent-free, direct printing of organic semiconductors in atmosphere", *Appl. Phys. Lett.* **2010**, *96*, 263301.

[12] Y. S. Tyan, "Organic light-emitting-diode lighting overview", *J. Photonics Energy* **2011**, *1(1)*, 011009.

[13] G. Horowitz, "Organic thin film transistors: from theory to real devices", *J. Mater. Res.* **2004**, *19*, 1946.

[14] B. P. Rand, J. Genoe, P. Heremans, J. Poortmans, "Solar cells utilizing small molecular weight organic semiconductors", *Prog. Photovoltaics: Res. Appl.* **2007**, *15*, 659.

[15] D. Yue, P. Khatav, F. You, S. B. Darling, "Deciphering the uncertainties in life cycle energy and environmental analysis of organic photovoltaics", *Energy Environ. Sci.* **2012**, *5*, 9163.

[16] A. Bernanose, M. Comte, P. Vouaux, "A new method of emission of light by certain organic compounds", *J. Chim. Phys.* **1953**, *50*, 64.

[17] W. Helfrich, W. G. Schneider, "Recombination radiation in anthracene crystals", *Phys. Rev. Lett.* **1965**, *14*, 229.

[18] C. W. Tang, S. A. VanSlyke, "Organic electroluminescent diodes", *Appl. Phys. Lett.* **1987**, *51*, 913.

[19] M. A. Baldo, D. F. O'Brien, Y. You, A. Shoustikov, S. Sibley, et al. "Highly efficient phosphorescent emission from organic electroluminescent devices'', *Nature* **1998**, *395*, 151.

[20] M. A. Baldo, S. Lamansky, P. E. Burrows, M. E. Thompson, S. R. Forrest, "Very high-efficiency green organic light-emitting devices based on electrophosphorescence", *Appl. Phys. Lett.* **1999**, *75*, 4.

[21] C. Adachi, M. A. Baldo, M. E. Thompson, S. R. Forrest, "Nearly 100% internal phosphorescence efficiency in an organic lightemitting device", *J. Appl. Phys.* **2001**, *90*, 5048.

[22] S. R. Forrest, D. D. C. Bradley, M. E. Thompson, "Measuring the efficiency of organic light-emitting devices", *Adv. Mater.* **2003**, *15(13)*, 1043.

[23] P. E. Burrows, Z. Shen, V. Bulovic, D. M. McCarty, S. R. Forrest, "Relationship between electroluminescence and current transport in organic heterojunction light emitting devices", *J. Appl. Phys.* **1996**, *79*, 7991.

[24] D. Kolosov, D. S. English, V. Bulovic, P. F. Barbara, S. R. Forrest, "Direct observation of structural changes in organic light emitting devices during degradation", *J. Appl. Phys.* **2001**, *90*, 3242.

[25] Z. D. Popovic, H. Aziz, A. Ioannidis, N. X. Hu, P. N. M. Anjos, "Long-term degradation mechanism of tris(8-hydroxyquinoline) aluminum-based organic light-emitting devices", *Synth. Metals* **2000**, *111—112*, 229.

[26] A. Yadav, Y. Jin, P. K. L. Chan, M. Shtein, K. P. Pipe, "Intermolecular electronic coupling in organic molecular thin films measured by temperature modulation spectroscopy", *Appl. Phys. Lett.* **2010**, *97*, 203307.

[27] C. D. Dimitrakopoulos, P. R. L. Malenfant, "Organic thin film transistors for large area electronics", *Adv. Mater.* **2002**, *14(2)*, 99.

[28] H. E. Katz, "Recent advances in semiconductor performance and printing processes for organic transistor-based electronics", *Chem. Mater.* **2004**, *16*, 4748.

[29] A. Facchetti, "Semiconductors for organic transistors", *Mater. Today* **2007**, *10*, 28.

[30] M. Kitamura, Y. Arakawa, "Pentacene-based organic field-effect transistors", *J. Phys.: Condens. Matter* **2008**, *20*, 184011.

[31] C. W. Tang, A. C. Albrecht, "Chlorophyll-*a* photovoltaic cells", *Nature* **1975**, *254*, 507.

[32] G. Yu, J. Gao, J. C. Hummelen, F. Wudl, A. G. Heeger, "Polymer photovoltaic cells: enhanced efficiencies via a network of internal donor-acceptor heterojunctions", *Science* **1995**, *270*, 1789.

[33] E. Tekin, P. J. Smith, U. S. Schubert, "Inkjet printing as a deposition and patterning tool for polymers and inorganic particles", *Soft Matter* **2008**, *4*, 703.

[34] P. Peumans, A. Yakimov, S. R. Forrest, "Small molecular weight organic thin-film photodetectors and solar cells", *J. Appl. Phys* **2003**, *93*, 3693.

[35] A. W. Hains, Z. Liang, M. A. Woodhouse, B. A. Gregg, "Molecular semiconductors in organic photovoltaic cells", *Chem. Rev.* **2010**, *110*, 6689.

[36] H. Hoppe, N. S. Sariciftci, "Organic solar cells: an overview", *J. Mater. Res.* **2004**, *19*, 1924.

[37] M. D. Perez, C. Borek, S. R. Forrest, M. E. Thompson, "Molecular and morphological influences on the open circuit voltages of organic photovoltaic devices", *J. Am. Chem. Soc.* **2009**, *131*, 9281.

[38] G. Wei, S. Wang, K. Renshaw, M. E. Thompson, S. R. Forrest, "Solution-processed squaraine bulk heterojunction photovoltaic cells", *ACS Nano* **2010**, *4(4),* 1927.

[39] J. Clark, G. Lanzani, "Organic photonics for communications", *Nat. Photonics* **2010**, *4*, 438.

[40] S. Chénais, S. Forget, "Recent advances in solid-state organic lasers", *Polymers Int.* **2012**, *61*, 390.

[41] I. D. W. Samuel, G. A. Turnbull, "Organic semiconductor lasers", *Chem. Rev.* **2007**, *107*, 1272.

[42] P. Peumans, V. Bulovic, S. R. Forrest, "Efficient, high-bandwidth organic multilayer photodetectors", *Appl. Phys. Lett.* **2000**, *76*, 3855.

[43] T. Morimune, H. Kajii, Y. Ohmori, "Photoresponse properties of a high-speed organic photodetector based on copperphthalocyanine under red light illumination", *IEEE Photonics Technol. Lett.* **2006**, *18*, 2662.

[44] J. C. Blakesley, P. E. Keivanidis, M. Campoy-Quiles, C. R. Newman, Y. Jin, et al. "Organic semiconductor devices for X-ray imaging", *Nucl. Instrum. Methods A* **2007**, *580*, 774.

[45] X. Xu, M. Davanco, X. Qi, S. R. Forrest, "Direct transfer patterning on three dimensionally deformed surfaces at micrometer resolutions and its application to hemispherical focal plane detector arrays", *Org. Electron.* **2008**, *9*, 1122.

[46] X. Xu, M. Mihnev, A. Taylor, S. R. Forrest, "Organic photodetector arrays with indium tin oxide electrodes patterned using directly transferred metal masks", *Appl. Phys. Lett.* **2009**, *94*, 043313.

[47] K. H. An, B. O'Connor, K. P. Pipe, Y. Zhao, M. Shtein, "Scanning optical probe microscopy with submicrometer resolution using an organic photodetector", *Appl. Phys. Lett.* **2008**, *93*, 033311.

[48] A. Pais, A. Banerjee, D. Klotzkin, I. Papautsky, "High-sensitivity, disposable lab-on-a-chip with thin-film organic electronics for fluorescence detection", *Lab Chip* **2008**, *8*, 794.

[49] J. R. Wojciechowski, L. C. Shriver-Lake, M. Y. Yamaguchi, E. Fureder, R. Pieler, et al. "Organic photodiodes for biosensor miniaturization", *Anal. Chem.* **2009**, *81*, 3455.

[50] E. L. Ratcliff, P. A. Veneman, A. Simmonds, B. Zacher, D. Huebner, et al. "A planar, chip-based, dual-beam refractometer using an integrated organic light-emitting diode (OLED) light source and organic photovoltaic (OPV) detectors", *Anal. Chem.* **2010**, *82*, 2734.

[51] M. R. Antognazza, U. Scherf, P. Monti, G. Lanzani, "Organic-based tristimuli colorimeter", *Appl. Phys. Lett.* **2007**, *90*, 163509.

[52] L. F. Cheng, L. S. Liao, W. Y. Lai, X. H. Sun, N. B. Wong, et al. "Effect of deposition rate on the morphology, chemistry and electroluminescence of tris-(8-hydroxyqiunoline) aluminum films", *Chem. Phys. Lett.* **2000**, *319*, 418.

[53] F. Yang, M. Shtein, S. R. Forrest, "Morphology control and material mixing by high-temperature organic vapor-phase deposition and its application to thin-film solar cells", *J. Appl. Phys.* **2005**, *98*, 014906.

[54] D. M. Price, "Vapor pressure determination by thermogravimetry", *Thermochem. Acta* **2001**, *367—68*, 253.

[55] T. Basova, P. Semyannikov, V. Plyashkevich, A. Hassan, I. Igumenov, "Volatile phthalocyanines: vapor pressure and thermodynamics", *Crit. Rev. Solid State Mater. Sci.* 2009, 34, 180.

[56] O. Shalev, M. Shtein, "Effect of crystal density on sublimation properties of molecular organic semiconductors", *Org. Electron.* **2013**, *14*, 94.

[57] R. Clausius, "Ueber die bewegende Kraft der Wärme und die Gesetze, welche sich daraus für die Wärmelehre selbst ableiten lassen", *Ann. Phys.* **1850**, *155*, 500.

[58] D. Kafer, M. E. Helou, C. Gemel, G. Witte, "Packing of planar organic molecules: interplay of van der Waals and electrostatic interaction", *Cryst. Growth Des.* **2008**, *8*, 3053.

[59] V. Oja, E. M. Suuberg, "Vapor pressures and enthalpies of sublimation of polycyclic aromatic hydrocarbons and their derivatives", *J. Chem. Eng. Data* **1998**, *43(3)*, 486.

[60] M. Rajeswaran, T. N. Blanton, C. W. Tang, W. C. Lenhart, S. C. Switalski, et al. "Structural, thermal, and spectral characterization of the different crystalline forms of Alq_3, tris(quinolin-8-olato)aluminum(III), an electroluminescent material in OLED technology", *Polyhedron* **2009**, *28*, 835.

[61] K. Yase, Y. Takahashi, N. Ara-Kato, A. Kawazu, "Evaporation rate and saturated vapor pressure of functional organic materials", *Jpn. J. Appl. Phys. Part 1* **1995**, *34*, 636.

[62] M. Shtein, P. Peumans, J. B. Benziger, S. R. Forrest, "Material transport regimes and mechanisms for growth of molecular organic thin films using low-pressure organic vapor phase deposition", *J. Appl. Phys.* **2001**, *89*, 1470.

[63] B. Krause, A. C. Dürr, K. A. Ritley, F. Schreiber, H. Dosch, D. Smilgies, "On the coexistence of different polymorphs in organic epitaxy: α and β phase of PTCDA on Ag(1 1 1)", *Appl. Surf. Sci.* **2001**, *175—76*, 332.

[64] M. K. Engel, “Single-crystal structures of phthalocyanine complexes and related macrocycles”, In *The Porphyrin Handbook*, ed. Kadish KM, Guilard R, **2003**, *20*. San Diego, CA: Academic

[65] H. Kietaibl, “Die Kristall- und Molekülstruktur eines neuratigen phthalocyaninähnlichen Borkomplexes”, *Monatsh. Fuer Chem.* **1974**, *105*, 405.

[66] H. Klauk, *Organic Electronics: Materials, Manufacturing, and Applications*. **2006**, Chapter 9.5. Weinheim: Wiley-VCH

[67] E. M. Tabernero, V. Martin, M. A. Galan, “Estimation of sublimation enthalpies of solids constituted by aromatic and/or polycyclic aliphatic rings by using a group contribution method”, *Am. Inst. Chem. Eng. J.* **2012**, *58*, 2875.

[68] D. Mathieu, “Simple alternative to neural networks for predicting sublimation enthalpies from fragment contributions”, *Ind. Eng. Chem. Res.* **2012**, *51*, 2814.

[69] H. J. Wagner, R. O. Loutfy, C. K. Hsiao, “Purification and characterization of phthalocyanines”, *J. Mater. Sci.* **1982**, *17*, 2781.

[70] H. Becker, I. Bach, M. Holbach, J. Schwaiger, H. Spreitzer, “Purity of OLED-materials and the implication on device performance”, *SID Symp. Dig. Tech. Papers* **2010**, *41*, 39.

[71] M. Pope, C. E. Swenberg, eds. *Electronic Processes in Organic Crystals*. Oxford: Clarendon Press, **1982**, 118.

[72] P. E. Burrows, V. Bulovic, S.R. Forrest, L. Sl. Sapochak, D. M. McCarty, M. E . Thompson, “Reliability and degradation of organic light emitting devices”, *Appl. Phys. Lett.* **1994**, *65*, 2922.

[73] M. Svhwoerer, H. C. Wolf, *Organic Molecular Solids*. Weinheim: Wiley-VCH, **2007**, 57.

[74] H. Klauk, *Organic Electronics: Materials, Manufacturing, and Applications*, **2006**, Chapter 9.4. Weinheim: Wiley-VCH.

[75] S. T. Lee, C. S. Lee, Z. Q. Gao, B. J. Chen, W. Y. Lai, T. C. Wong, "Performance optimization of organic electroluminescent devices", *Proc. SPIE Org. Light-Emit. Mater. Devices III* **1999**, *3797*, 138.

[76] S. B. Rim, R. F. Fink, J. C. Schöneboom, P. Erk, P. Peumans, "Effect of molecular packing on the exciton diffusion length in organic solar cells", *Appl. Phys. Lett.* **2007**, *91*, 173504.

[77] J. Xue, S. Uchida, B. P. Rand, S. R. Forrest, "Asymmetric tandem organic photovoltaic cells with hybrid planar-mixed molecular heterojunctions", *Appl. Phys. Lett.* **2004**, *85*, 5757.

[78] P. Peumans, S. Uchida, S. R. Forrest, "Efficient bulk heterojunction photovoltaic cells using small-molecular-weight organic thin films", *Nature* **2003**, *425*, 158.

[79] R. Pandey, A. A. Gunawan, K. A. Mkhoyan, R. J. Holmes, "Efficient organic photovoltaic cells based on nanocrystalline mixtures of boron subphthalocyanine chloride and C_{60}", *Adv. Funct. Mater.* **2012**, *22*, 617.

[80] S. R. Forrest, "Ultrathin organic films grown by organic molecular beam deposition and related techniques", *Chem. Rev.* **1997**, *97*, 1793.

[81] W. Gao, A. Kahn, "Electrical doping: the impact on interfaces of π-conjugated molecular films", *J. Phys.: Condens. Matter* **2003**, *15*, S2757.

[82] Q. Zhang, T. Atay, J. R. Tischler, M. S. Bradley, V. Bulovic, A. V. Nurmikko, "Highly efficient resonant coupling of optical excitations in hybrid organic/inorganic semiconductor nanostructures", *Nat. Nanotechnol.* **2007**, *2*, 555.

[83] S. Blumstengel, S. Sadofev, J. Puls, F. Henneberger, "An inorganic/organic semiconductor "sandwich" structure grown by molecular beam epitaxy", *Adv. Mater.* **2009**, *21*, 4850.

[84] L. Kilian, E. Umbach, M. Sokolowski, "Molecular beam epitaxy of organic films investigated by high resolution low energy electron diffraction (SPA-LEED): 3,4,9,10-perylenetetracarboxylicacid-dianhydride (PTCDA) on Ag(111)", *Surf. Sci.* **2004**, *573*, 359.

[85] L. Kilian, A. Hauschild, R. Temirov, S. Soubatch, A. Scholl, et al. "Role of intermolecular interactions on the electronic and geometric structure of a large π-conjugated molecule adsorbed on a metal surface", *Phys. Rev. Lett.* **2008**, *100*, 136103.

[86] N. Koch, "Organic electronic devices and their functional interfaces", *ChemPhysChem* **2007**, *8*, 1438.

[87] I. G. Hill, D. J. Milliron, A. Kahn, "Organic semiconductor interfaces: electronic structure and transport properties", *Appl. Surf. Sci.* **2000**, *166*, 354.

[88] A. I. Kitaigorodsky, *Molecular Crystals and Molecules*. New York: Academic. **1973**, 553.

[89] E. A. Silinsh. V. Capek. *Organic Molecular Crystals: Interaction, Localization, and Transport Phenomena*. New York: Am. Inst. Phys. **1994.**

[90] M. Shtein,. Organic vapor phase deposition. In *Organic Electronics*, ed. F So, **2010**, 27, New York: CRC Press.

[91] R. B. Bird, W. E. Stewart, E. N. Lightfoot, *Transport Phenomena*, **2002**, 513, New York: John Wiley & Sons. 920 pp.

[92] J. C. Slattery, R. B. Bird, "Calculation of the diffusion coefficient of dilute gases and of the self-diffusion coefficient of dense gases", *Am. Inst. Chem. Eng. J.* **1958**, *4*, 137.

[93] T. R. Marrero, E. A. Mason, "Gaseous diffusion coefficients", *J. Phys. Chem. Ref. Data* **1972**, *1*, 3.

[94] T. X. Zhou, T. Ngo, J. J. Brown, M. Shtein, S. R. Forrest, "Stable and efficient electrophosphorescent organic light-emitting devices grown by organic vapor phase deposition", *Appl. Phys. Lett.* **2005**, *86*, 021107.

[95] C. Calí, V. Daneu, A. Orioli, S. Riva-Sanseverino, "Flash evaporation of compounds with a pulsed-discharge CO_2 laser", *Appl. Opt.* **1976**, *15*, 1327.

[96] Y. S. Tyan, M. Long, G. M. Phelan, T. R. Cushman,. Vapor deposition apparatus and method, **2007**, *US Patent No. 20070098891.*

[97] M. Long, B. E. Koppe, N. P. Redden, M. L. Boroson, T. K. Hatwar, J. W. Hamer, "Enabling high- throughput, low-cost manufacturing of OLED display and lighting panels", *MRS Proc*. **2009**, *1212*, 1212–S06- 06-C07-06.

[98] J. D. Zimmerman, X. Xiao, C. K. Renshaw, S. Wang, V. V. Diev, et al. "Independent control of bulk and interfacial morphologies of small molecular weight organic heterojunction solar cells", *Nano Lett.* **2012**, *12*, 4366.

[99] D. Yokoyama, "Molecular orientation in small-molecule organic light-emitting diodes", *J. Mater. Chem.* **2011**, *21*, 19187.

[100] M. Shtein, J. Mapel, J. B. Benziger, S. R. Forrest, "Effects of film morphology and gate dielectric surface preparation on the electrical characteristics of organic-vapor-phase- deposited pentacene thin-film transistors", *Appl. Phys. Lett.* **2002**, *81*, 268.

[101] F. Yang, S. R. Forrest, "Photocurrent generation in nanostructured organic solar cells", *ACS Nano* **2008**, *2*, 1022.

[102] H. W. Kang, C. Yun, S. Yoo, S. H. Ko, H. J. Sung, "Effect of carrier gas temperature on pentacene thin film formation by organic vapor-jet printing techniques", *Thermochim. Acta* **2012**, *542*, 74.

[103] C. Py, D. Roth, I. Lévesque, J. Stapledon, A. Donat-Bouillud, "An integrated shadow-mask based on a stack of inorganic insulators for high-resolution OLEDs using evaporated or spun-on materials", *Synth. Metals* **2001**, *122*, 225.

[104] C. W. Tang, K. C. Pan, "A full color active matrix organic electroluminescent display panel having an integrated shadow mask", **2002**, *US Patent No. 6384529*.

[105] F. P. Baude, "Method of making full color display panels", **2007**, *Eur. Patent No. 1399967 B1*.

[106] M. Shtein, P. Peumans, J. B. Benziger, S. R. Forrest, "Micropatterning of small molecular weight organic semiconductor thin films using organic vapor phase deposition", *J. Appl. Phys.* **2003**, *93*, 4005.

[107] J. Chen, V. Leblanc, S. H. Kang, M. A. Baldo, P. J. Benning, et al. "Direct patterning of molecular organic materials and metals using a micromachined printhead", *Mater. Res. Soc. Symp. Proc.* **2005**, *870*, H1.8.

[108] J. Chen, V. Leblanc, S. H. Kang, P. J. Benning, D. Schut, et al. "High definition digital fabrication of active organic devices by molecular jet printing", *Adv. Funct. Mater.* **2007**, *17*, 2722.

[109] V. Leblanc, J. Chen, S. H. Kang, V. Bulovic, M. A. Schmidt, "Micromachined printheads for the evaporative patterning of organic materials and metals", *J. Microelectromech. Syst.* **2007**, *16*, 394.

[110] C. G. Courcimault, M. G. Allen, "Reconfigurable shadow mask technology: a microsystem for metal nanoline deposition", *Nanotechnology* **2004**, *15*, S528—33.

[111] H. Sirringhaus, T. Kawase, R. H. Friend, T. Shimoda, M. Inbasekaran, et al. "High-resolution inkjet printing of all-polymer transistor circuits", *Science* **2000**, *290*, 2123.

[112] C. J. Drury, C. M. J. Mutsaers, C. M. Hart, M. Matters, D. M. de Leeuw, "Low-cost all-polymer integrated circuits", *Appl. Phys. Lett.* **1998**, *73*, 108.

[113] T. R. Hebner, C. C. Wu, D. Marcy, M. H. Lu, J. C. Sturm, "Ink-jet printing of doped polymers for organic light emitting devices", *Appl. Phys. Lett.* **1998**, *72*, 519.

[114] M. Singh, H. M. Haverinen, P. Dhagat, G. E. Jabbour, "Inkjet printing---process and its applications", *Adv. Mater.* **2010**, *22*, 673.

[115] C. Wu, C. Yang, H. Chang, W. Chen, C. Lee, "Finite-source dye-diffusion thermal transfer for doping and color integration of organic light-emitting devices", *Appl. Phys. Lett.* **2000**, *77*, 794.

[116] J. A. Rogers, Z. Bao, K. Baldwin, A. Dodabalapur, B. Crone, et al. "Paper-like electronic displays: large-area rubber-stamped plastic sheets of electronics and microencapsulated electrophoretic inks", *Proc. Natl. Acad. Sci. USA* **2001**, *98*, 4835.

[117] J. Zaumseil, T. Someya, Z. Bao, Y-L. Loo, R. Cirelli, J. A. Rogers, "Nanoscale organic transistors that use source-drain electrodes supported by high resolution rubber stamps", *Appl. Phys. Lett.* **2003**, *82*, 793.

[118] C. Kim, P. E. Burrows, S. R. Forrest, "Micropatterning of organic electronic devices by cold-welding", *Science* **2000**, *288*, 831.

[119] C. Kim, M. Shtein, S. R. Forrest, "Nanolithography based on patterned metal transfer and its application to organic electronic devices", *Appl. Phys. Lett.* **2002**, *80*, 4051.

[120] G. B. Blanchet, Y. L. Loo, J. A. Rogers, F. Gao, C. R. Fincher, "Large area, high resolution, dry printing of conducting polymers for organic electronics", *Appl. Phys. Lett.* **2003**, *82*, 463.

[121] Y. J. Lee, S. T. Lee, "Laser-induced thermal imaging of polymer light-emitting materials on poly(3,4-ethylenedioxythiophene): silane hole-transport layer", *Adv. Mater.* **2004**, *16*, 51.

[122] S. Lamansky, T. R. Hoffend, H. Le, V. Jones, M. B. Wolk, W. A. Tolbert, "Laser induced thermal imaging of vacuum-coated OLED materials", *Proc. SPIE Org. Light-Emit. Mater. Devices IX*, **2005**, *5937*, 593702.

[123] G. A. Bird,. "Monte Carlo simulation of gas flows", *Annu. Rev. Fluid Mech.* **1978**, *10*, 11.

[124] M. Shtein, P. Peumans, J. B. Benzinger, S. R. Forrest, "Direct mask-free patterning of molecular organic semiconductors using organic vapor jet printing", *J. Appl. Phys.* **2004**, *96*, 4500.

[125] Y. Sun, M. Shtein, S. R. Forrest, "Direct patterning of organic light-emitting devices by organic-vapor jet printing", *Appl. Phys. Lett.* **2005**, *86*, 113504.

[126] M. S. Arnold, G. J. McGraw, S. R. Forrest, R. R. Lunt, "Direct vapor jet printing of three color segment organic light emitting devices for white light illumination", *Appl. Phys. Lett.* **2008**, *92*, 053301.

[127] G. J. McGraw, D. L. Peters, S. R. Forrest, “Organic vapor jet printing at micrometer resolution using microfluidic nozzle arrays”, *Appl. Phys. Lett.* **2011**, *98*, 013302.

[128] G. J. McGraw, S. R. Forrest, “Fluid dynamics and mass transport in organic vapor jet printing”, *J. Appl. Phys.* **2012**, *111*, 043501.

[129] C. Yun, C. Jungmin, H. W. Kang, M. Kim, H. Moon, et al. “Digital-mode organic vapor-jet printing (D-OVJP): advanced jet-on-demand control of organic thin-film deposition”, *Adv. Mater.* **2012**, *24*, 2857.

[130] S. Biswas, K. A. Luck, M. Shtein, “Guard flow-enhanced organic vapor jet printing of photovoltaic donor materials in air”, *Org. Electron.* **2012**, *13*, 2905.

[131] S. Biswas, Y. Yang, C. M. Schlepütz, N. Geva, R. L. Headrick, R. Pindak, R. Clarke and M. Shtein, "Spatial mapping of morphology and electronic properties of air-printed pentacene thin films”, *Adv. Funct. Mater.*, **2014**, (*accepted, in print*).